scientific reports

Check for updates

OPEN

A non-stationary bias adjustment method for improving the inter-annual variability and persistence of projected precipitation

Marina Cantalejo, Manuel Cobos ✉, Agustín Millares & Asunción Baquerizo

Hydrological studies depend heavily on environmental variables, such as precipitation and resulting runoff, which exhibit highly seasonal and intermittent behaviour in semiarid basins. In these basins, the use of traditional methods to adjust biases in time series projections can lead to inaccurate results regarding the impacts of climate change. This study introduces a non-stationary bias adjustment methodology (NS) specifically designed for environmental variables characterized by sporadic events and substantial intensity variability, such as precipitation. The methodology involves establishing a probability threshold to adapt the occurrence of precipitation events and utilizes a quantile mapping method based on a non-stationary theoretical and parametric distribution to adjust biases associated with precipitation intensity. The NS method is applied to daily precipitation projections from seven regional climatic models under the RCP 8.5 scenario spanning 2006–2100, alongside historical concurrent data from 1970 to 2005. The present method is compared to the widely used quantile delta mapping approach (QDM), revealing significant differences in performance related to the distribution of precipitation events throughout the year and the behaviour of mean and extreme intensity values. Both approaches show reliable performance, with root mean square errors between the empirical distribution functions of the corrected hindcast time series and the observations being lower than or close to 1 mm for the percentiles smaller than 50th. The error increases with the percentiles, particularly at stations located at higher altitudes. In these locations, QDM doubles or triples the error obtained with the non-stationary approach for percentiles higher than 75th, reaching up to 34 mm. The proposed methodology demonstrates promising potential in reducing uncertainties associated with systematic errors in inter-annual precipitation variability. It is a first step to jointly apply a similar approach to all involved driving variables. Such methods are key to assessing hydrological responses and associated impacts in semi-arid mountainous basins all around the Globe.

Keywords Non-stationary bias, Quantile mapping, Interannual variability, Climate change, Uncertainty

Regional climate models (RCMs) have been widely used for hydrological and water resources impact assessments during the last decade[1–3]. This kind of dynamical downscaling procedures provide a good description of orographic effects and mesoscale patterns[4–6]. However, atmospheric models have structural errors and parameterizations that affect their ability to predict the spatiotemporal behaviour of precipitation[7–10] and limit the modelling of climate variability at regional and local scales. Most RCM models present limitations to capture the representative local scale climate patterns[11–13] or the regional variability at inter-annual to decadal time scales[8,14–17]. Convection permitting models, with finer resolutions ($\lesssim 4$ km), resolve convective processes and improve regional and local-scale climate information, however, they face significant future challenges such as the lack of reliable high temporal and spatial resolution observations, the large data volume generated and the heavy computational requirements[18,19]. These difficulties are relevant to precipitation over areas with complex topography and high spatial and temporal variability[20,21]. The bias of RCMs complicates the assessment of runoff at places that are strongly influenced by small-scale precipitation patterns[17], characteristic of mountainous environments[22,23] and semi-arid regions[24] where intermittency and spring-flooding events have a significant hydrological impact during the thawing period in snowmelt driven basins[17,25,26].

Environmental Fluid Dynamics Group, Andalusian Institute for Earth System Research (IISTA), Avda. del Mediterráneo s/n 18006, Granada, Spain. ✉email: mcobosb@ugr.es

Works found in the literature commonly employ two statistical corrections that utilize two reference series to formulate the correction function used in the projection. One series is derived from observations and the other from modelling. These corrections include (i) adjustment of the frequency of event occurrence and (ii) correction of magnitude biases[27,28]. The former is necessary when there is a significant difference between the precipitation occurrences of the reference series, typically observed when the temporal series' time step is daily or sub-daily. The latter assumes that the bias remains consistent for both the historical period and projections. These disparities present challenges for accurate correction, given their intermittence and the crucial persistence associated with their occurrence or absence[29]. The present study is also founded on these premises to develop a two-step non-stationary (NS) bias adjustment method.

There are several ways to perform the occurrence bias adjustment of precipitation, for instance, (i) by preserving the wet-dry ratio of the observed period under the assumption that the climate models produce the same number of raining days[30], (ii) by partially correcting the wet days[31], (iii) by direct approach[32,33], through maintaining a minimum threshold as in the observed period[34], adapting the threshold to ensure the same frequency days of precipitation[35], or (iv) by partially correcting the dry days[29]. When hindcast data, which are the modelling results for the historical period, have more wet days than observations, it appears the so-called "drizzle effect" or drizzle days[30,36,37]. Conversely, the "drier effect" appears when the modelled data underestimate the precipitation occurrence for the period under observation. For these cases, Themeβi et al.[37] proposed a frequency adaptation method. Piani et al.[9] suggested to retain the dry and drizzle statistics in the transfer function between the simulated and corrected variable. Vrac et al.[29] successfully validated a methodology for adjusting occurrence by replacing zero precipitation values with a uniform random distribution below the minimum observation threshold. In basins where the interannual behaviour of precipitation is highly variable; it is convenient to address both phenomena with a NS adjustment of the threshold.

The second correction step focus on the bias of the magnitude of interest. Recent inter-comparison works have analysed the performance of different univariate and multivariate bias adjustment methods for adjusting the bias of variables such as precipitation and temperature[34,38–44]. Most of them focused on the quantile mapping method proposed by Panofsky et al.[45] (see also Déqué et al.[46] for further information) and the recent developments of the detrended quantile mapping and quantile delta mapping (QDM)[34]. All these methodologies have been widely used due to their flexibility and simplicity[47–51]. The quantile mapping method shows the ability to preserve the climate signal along the 21st century[34,52–54], however, the climate distribution might significantly change over time neglecting the stationarity premise[55–57].

The methods based on the quantile mapping and the QDM require the estimation of the distribution functions of precipitation intensity. In that regard, Gudmundsson et al.[58] pointed out that parametric approaches are usually site specific. However, the use of non-parametric ones makes it difficult to capture extreme values behaviour and, as observed by Michelangeli et al.[59], their use for projections is only valid for the range of values of observations.

Some works indicate that the model bias is time-dependent and related to the dynamic feedback of climate processes[41,44,52,60,61]. The study proposed by Miao et al.[53] formulated a mix of conditional transformations for gamma and beta distributions for independently removing monthly or seasonal NS bias of temperature and precipitation. However, such distributions, may not be suitable for all studies involving precipitation, especially with respect to extremes[62].

Some of the above-mentioned methodologies are susceptible to be modified to consider non stationarity, thereby elevating the level of certainty associated with future impacts[28,63]. The approach can be done, in principle, by dividing the time interval into subintervals (i.e. the year into seasons or months). From a practical point of view, however, it is required that (i) the number of data values in the month or season is long enough to adequately characterize high percentiles; (ii) the parameterization of the distribution function changes gradually between divisions. In arid or semiarid regions like the study area, the precipitation exhibits high intermittency, which means months even without rainy days, and a highly seasonal behaviour, which shows strong changes between distributions, that makes such a non-stationary approach unaffordable.

The present study introduces a methodology based on the QDM method, utilizing a NS parametric theoretical distribution function to preserve the bias of the historical period in projections of univariate variables. This methodology has been applied at an inter-annual scale to precipitation at a semi-arid study site in the southeast of the Iberian Peninsula, where precipitation exhibits high spatial and temporal variability, as well as pronounced seasonality and intermittency of events. This is a key first step in understanding future hydrological scenarios. Specifically, this approach: (i) does not require extrapolation techniques for values beyond the calibration period range, (ii) does not impose any theoretical probability model, (iii) does not correct extreme events independently, and (iv) is capable of removing bias across different time scales, from days to decades. It should be noted that the method has a general character and can, therefore, be applied to other univariate variables as well.

The paper is organised as follows. In Sect. 2, the study site and available data are presented. Section 3 describes the NS coupled correction method and highlights the relevance of the NS approach. Section 4 presents the advantages of the proposed methodology through a comparison to the QDM technique. Section 5 discusses the results, and the conclusion completes the manuscript.

Data

Study site

The mountainous basin of the Guadalfeo River is situated at the southeastern Iberian Peninsula, covering an area of 1250 km^2 (Fig. 1). The hydrological dynamics and pluvio-nival character of this small Mediterranean semi-arid basin are governed by the influence of the Sierra Nevada Mountain (Spain). Over the past 30 years, a monitoring network deployed in the basin has provided hydro-meteorological data[64]. The mean annual precipitation in the basin from 1970 to 2005 was 603 mm, with minimum and maximum values of 380 mm and

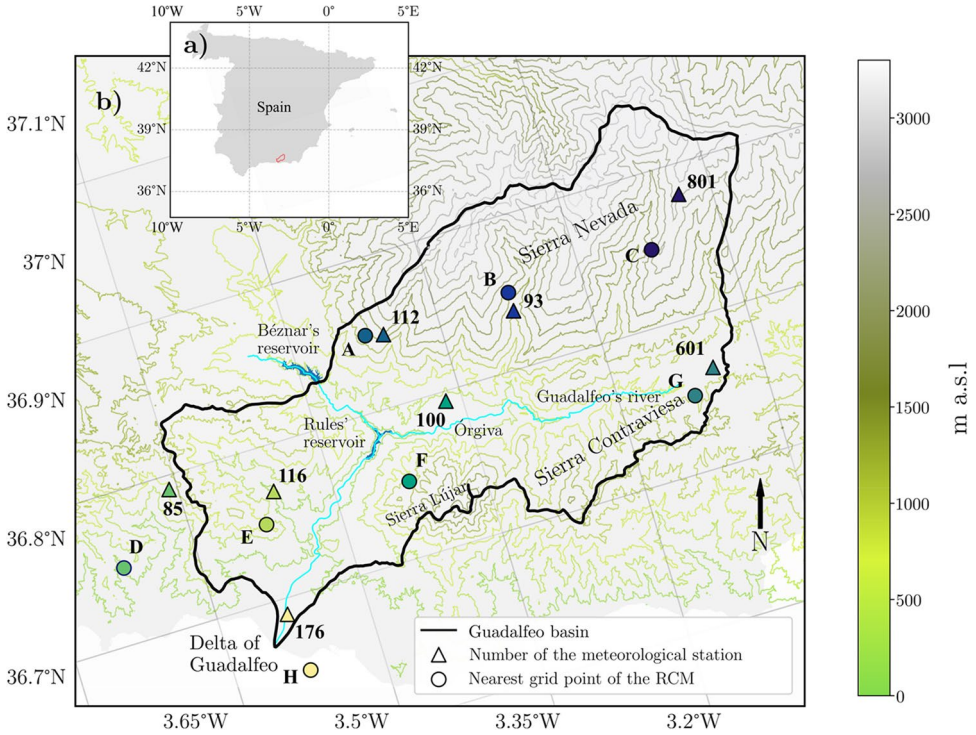

Fig. 1. Location of the study site and data sources. **a**) Location of the Guadalfeo river basin (southern Spain). **b**) Distribution of meteorological stations (triangles) and their nearest grid points of RCMs (circles). The map is created using the Python Matplotlib library[66]. The contour lines are obtained from the Digital Terrain Model (DTM) with a 25 m grid pitch from LiDAR 2014–2015 flights, in Spanish called MDT25 and distributed by the Spanish National Centre for Geographic Information (CNIG)[67]. The river and reservoir information are obtained from the Structures, Hydrography, and Urban System layers of the Andalusian Environmental Network (DERA)[68]. The map uses EPSG:4326 coordinates with a geographic coordinate grid. The grid of the RCM models is also shown with grey lines.

986 mm, respectively. Precipitation exhibits a significant altitude gradient, with mean annual values ranging from approximately 420 mm near the coast to 497–558 mm at Órgiva (450 m a.s.l.) and Contraviesa mountains (1500 m a.s.l.), respectively. It increases to 739 mm at Sierra Nevada (2470 m a.s.l.), located approximately 40 km from the coast. Above 2000 m altitude, more than 75% of the total annual precipitation occurs as snow[65].

The study region faces significant changes in meteorological factors when considering climate projections for Mediterranean environments[69,70]. Specifically, results from the European branch of the international project Coordinated Regional Climate Downscaling Experiment (EURO-CORDEX) predict a mean precipitation drop of 20% over the Iberian Peninsula for the end of the 21st century which was not evenly distributed throughout the year. In fact, the decrease in the number of heavy precipitation events is projected to be close to 15% in summer, while an increase up to 25% is expected during other times of the year. These changes have implications for hydrological processes, such as water availability in reservoirs[71] and erosive and sedimentary processes[64,72].

Available data

Daily precipitation measurements were obtained from meteorological stations located at various altitudinal environments, ranging from 50 to 2500 m above sea level (m a.s.l.) (Table 1). These stations are strategically positioned to assess the spatial distribution of hydro-meteorological drivers, altitudinal gradients, and snow dynamics in the Sierra Nevada mountains (Spain)[64]. The records span over the selected study period, from 1970 to 2005. Stations #100, #601 and #801 were analysed and compared with nearby stations to complete the precipitation series according to their spatial and altitudinal distribution[70]. Their good assessment of local meteorological and hydrological behaviour was confirmed by different research works[65,73–76].

This information was utilized in conjunction with a set of dynamically downscaled climate mean daily precipitation data obtained from various global and regional climate models (GCM-RCM) under the RCP 8.5 scenario, which have continuity in the so called SSP5-8.5 of the more recent Shared Socioeconomic Pathways scenario[77]. The historical and projected periods range 1970–2005 and 2006–2100, respectively. These time series are derived from EURO-CORDEX initiative which provides hindcast data for the historical period (hereinafter referred to as hindcast) and projections for worldwide regions according to the Fifth Assessment Report[78], utilizing a daily temporal resolution and a regular grid with a spatial resolution of 0.11° (approximately 12.5 km).

We utilized the results of the RCMs of the Danish Meteorological Institute (DMI), the Royal Netherland Meteorological Institute (KNMI) and the Swedish Meteorological and Hydrological Institute (SMHI) (Table 2, see Sobolowski et al.[79] for further information). These models have been previously used for the analysis of

Station #	Altitude [m]	Longitude	Latitude	Source of information	Toponymy
176 (H)	50	-3.567 (-3.546)	36.746 (36.706)	AEMET[1]	Salobreña
116 (E)	262	-3.580 (-3.586)	36.835 (36.811)	AEMET	Guájar-Fondón
100 (F)	450	-3.424 (-3.457)	36.901 (36.784)	AEMET	Órgiva
85 (D)	631	-3.674 (-3.714)	36.837 (36.779)	AEMET	Lentegí
601 (G)	950	-3.183 (-3.199)	36.925 (36.904)	RIA-IFAPA[2]	Cádiar
93 (B)	1530	-3.363 (-3.367)	36.966 (36.979)	AEMET	Poqueira
112 (A)	1652	-3.480 (-3.496)	36.949 (36.947)	AEMET	Arquilla
801 (C)	2470	-3.214 (-3.238)	37.050 (36.009)	UGR/UCO[3]	Tajos de Breca

Table 1. Information on meteorological stations. Parentheses indicate information from RCM grid points. [1]Meteorological National Agency. [2]Regional Agroclimatic network. [3]Universities of Granada and Cordoba.

Institute	Driving Model	RCM	Domain	Time Freq. (h)	Temporal Coverage	Version	Ensemble
DMI	ICHEC-EC-EARTH	HIRHAM5	EUR-11	3	1970–2005 2006–2100	20,190,926	r1i1p1
DMI	NCC-NorESM1-M	HIRHAM5	EUR-11	3	1970–2005 2006–2100	20,190,926	r1i1p1
KNMI	ICHEC-EC-EARTH	RACMO22E	EUR-11	3	1970–2005 2006–2100	20,200,901	r1i1p1
SMHI	CNRM-CERFACS-CNRM-CM5	RCA4	EUR-11	3	1970–2005 2006–2100	20,150,421	r1i1p1
SMHI	IPSL-IPSL-CM5A-MR	RCA4	EUR-11	3	1970–2005 2006–2100	20,150,421	r1i1p1
SMHI	MPI-M-MPI-ESM-LR	RCA4	EUR-11	3	1970–2005 2006–2100	20,191,116 20,160,803	r2i1p1 r1i1p1
SMHI	NCC-NorESM1-M	RCA4	EUR-11	3	1970–2005 2006–2100	20,180,820	r1i1p1

Table 2. RCM experiments used in the present study.

precipitation projections in Mediterranean basins[80,81] and fit both the spatial and temporal resolution as well as the available data at the study area.

Methodology

We begin with daily precipitation time series of observations and RCM data covering the same historical period (1970–2005) for which there is available information of observations and hindcast data and projected for the future period 2006–2100 with the selected GCM-RCM models (see Sect. 2.2), denoted as $x_o(t)$, $x_h(t)$, and $x_p(t)$, respectively, where *t* represents time.

The proposed coupled NS method corrects the bias of the projections in two steps: adjusting of precipitation frequency first and correcting the bias in the amount of precipitation by means of a NS quantile delta mapping adjustment technique. The steps of the methodology are outlined in Fig. 2 and summarized below.

For each station, a series of observed precipitation data, a corresponding hindcast series, and a projection are available at the stations given in Table 1. The following bias correction procedure is applied to each station:

- The observations, x_o(t), and hindcast data, x_h(t), are analysed using empirical distribution function to establish a non-stationary wet-day threshold, $x_h^*(t)$ (Sect. 3.1). The use of this threshold to select precipitation data in the hindcast series ensures that the same number of precipitation days is present in both the observed and hindcast series. Within this step, an occurrence corrected hindcast (OC-H) series is obtained.
- The observed and corrected hindcast series are analysed using a non-stationary parametric statistical model, resulting in the definition of the corresponding non-stationary distribution functions, F_o and F_h (Sect. 3.2). The difference between these functions lead to the transfer function, T, which relates the precipitation value before and after correction for a given point in time and probability values.
- The bias adjusted hindcast (BA-H) series, x_h^{NS}, along with the observations, x_o, are used to assess the performance of the method (Sect. 3.3).

Finally, the application of the correction procedure for timeseries of projections follows the next steps:

- The projected values that exceed the non-stationary threshold ($x_h^*(t)$) are neglected, resulting in the corrected series (OC-P).
- The transfer function is applied to OC-P using the NS parametric distribution fitted to the corrected projection series (F_p), yielding the bias adjusted timeseries of projections (BA-P).

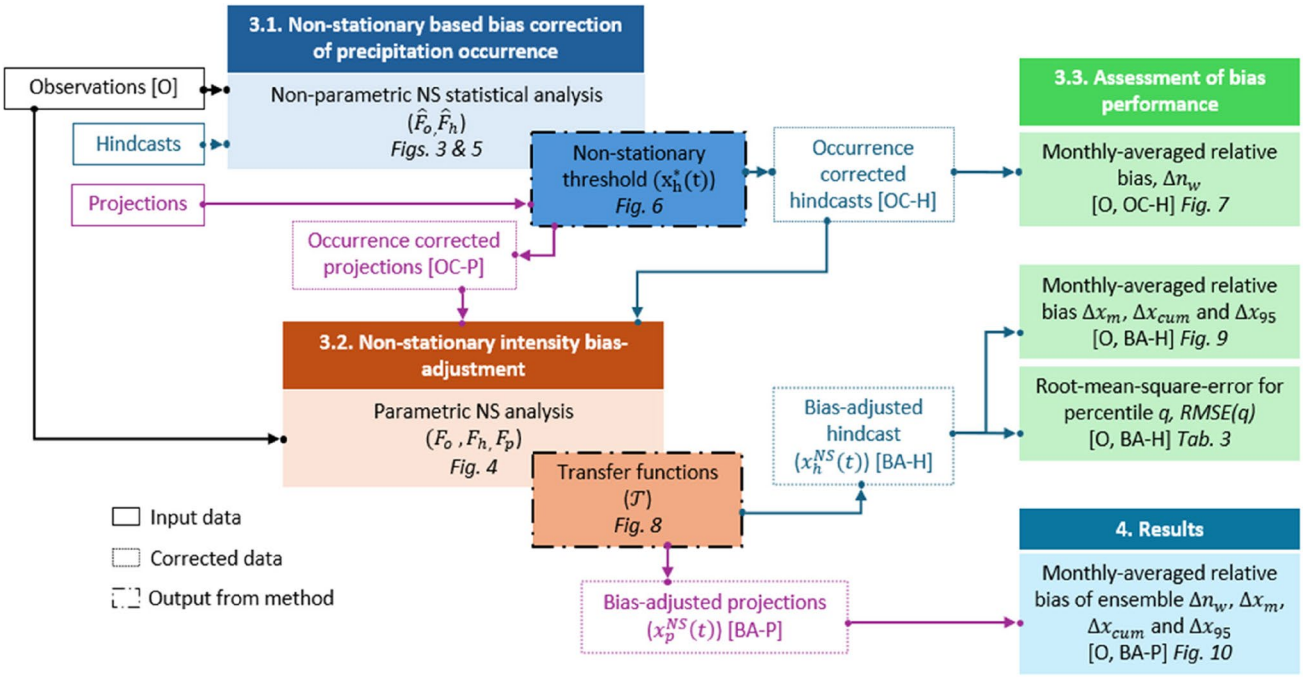

Fig. 2. Flowchart illustrating the steps for the application and the assessment of the proposed NS method.

The non-stationary character of precipitation is considered by means of a NS cumulative distribution function ($F(x;t)$) that estimates the non-exceedance probability of value x at a certain day t that varies over a selected time interval, I. The choice of I depends on the length of the time series available and the scales that want to be analysed, such as the yearly and inter-annual, among others, all related to climate variations[82]. In the application shown in Sect. 3.1 for the precipitation frequency and in Sect. 3.2 for the precipitation magnitude, the correction is done taking I as the year and allows to analyse the variability at scales shorter than and equal to the yearly one. As detailed in Cobos et al.[82] the NS distribution function is defined in terms of time dependent parameters that are expressed as truncated generalized Fourier expansions and which coefficients are fit to observations by means of the maximum likelihood method[83,84]. This approach allows to capture the time dependence in a global way. More information about the fitting methodology can be found in the Supplementary Material (SM).

Non-stationary based bias correction of precipitation occurrence

The analysis of precipitation frequency starts with the set-up of a wet-day threshold from observations, x_o^*. In the literature, this threshold is usually taken as a constant value varying from $x_o^* = 0.1$ mm/day[58,85–87] to $x_o^* = 1$ mm/day[88]. Different procedures are recommended to pre-process data depending on whether the well-known drizzling effect[36] or drying problem[37,89] occurs. For our study area a minimum amount of precipitation that can be registered, $x_o^* = 0.1$ mm/day, is selected.

The NS approach for occurrence-bias adjustment implies the computation of the empirical F for hindcast $\left(\hat{F}_h\right)$ and observations $\left(\hat{F}_o\right)$.

The procedure begins by replacing all values that fulfil $x_h(t) < x_o^*$ by uniform random values between zero and x_o^*, as in the singularity stochastic removal method[29]. Then, the hindcast values below a NS threshold (i.e., time varying value) as defined in Eq. (1) are neglected:

$$x_h^*(t) = \hat{F}_h^{-1}\left(\hat{F}_o(x_o^*;\, t)\,;\, t\right) \tag{1}$$

where superscript -1 refers to the inverse of the distribution function. With this approach, at time t, hindcast and observed data contain the same proportion of values over the threshold. This procedure addresses both drizzling and drier effects in the correction of the occurrence of precipitation. Regarding the drier effect ($\hat{F}_h(x_o^*;t) > \hat{F}_o(x_o^*;\, t)$), the present study is consistent with the work by Ines and Hansen[85] and Themeßi et al.[37], and those randomly generated values below the NS threshold, $x_h^*(t)$, are neglected. Where drizzling effect occurs at t, $\hat{F}_h(x_o^*;t) < \hat{F}_o(x_o^*;\, t)$, all the randomly generated values are neglected.

Figure 3 shows $\hat{F}_o(x_o^*;t)$ for observations, $\hat{F}_h(x_o^*;t)$ for hindcast data, using in both cases the observed threshold (0.1 mm/day), and $\hat{F}_h(x_h^*(t)\,;t)$ for hindcast data considering the new NS threshold for the model SMHI-IPSL-IPSL-CM5A-MR at station #176, all of them computed with a centred moving window of 14 days-length. It can be observed that the time series primarily presents drizzle days (e.g., winter season with upside arrow) alternating with drier days throughout the year (downside arrows). After the selection of the computed NS threshold $x_h^*(t)$, $\hat{F}_h(x_h^*(t)\,;t)$ and $\hat{F}_o(x_o^*;t)$ match perfectly (thicker green line).

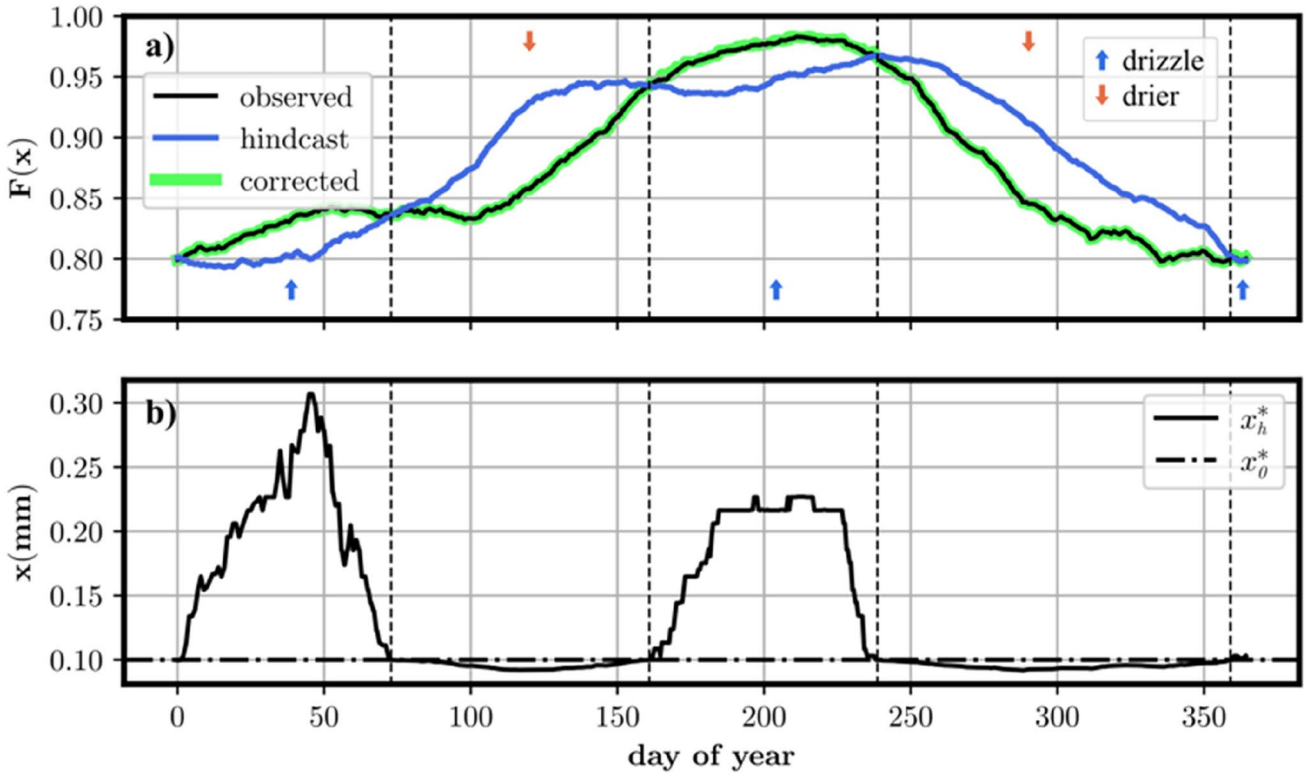

Fig. 3. Non-stationary occurrence-bias-adjustment. **a**) Non-exceedance probabilities $\widehat{F}_o\left(x_o^*\right)$ (black solid line), $\widehat{F}_h\left(x_o^*;t\right)$ (blue solid line) and occurrence-bias corrected $\widehat{F}_h\left(x_h^*\left(t\right);t\right)$ (thicker green solid line) along the year for the model SMHI-IPSL-IPSL-CM5A-MR at station #176. The arrows indicate where drizzle (upside) and

Non-stationary correction of precipitation magnitude

After applying the NS occurrence-bias-adjustment, the QDM is employed using theoretical NS parametric probability models tailored to observed, hindcast and projected datasets. The NS quantile delta mapping reads:

$$x_\xi^{NS}\left(t\right)=x_\xi\left(t\right)+\mathcal{T}\left(F_\xi\left(x_\xi\left(t\right);t\right)\right) \tag{2}$$

where

$$\mathcal{T}\left(F_\xi\left(x_\xi\left(t\right);t\right)\right)=F_o^{-1}\left(F_\xi\left(x_\xi\left(t\right);t\right)\right)-F_h^{-1}\left(F_\xi\left(x_\xi\left(t\right);t\right)\right). \tag{3}$$

In Eqs. (2) and (3), $F_o(x_p\left(t\right);t)$ and $F_h(x_p\left(t\right);t)$ represent the cumulative distribution functions of observed and hindcast data, respectively. The subscript $\xi = h\ or\ p$ on $F_\xi\left(x_\xi\left(t\right);t\right)$ denotes the distribution function of hindcast or projected data, and on $x_\xi^{NS}\left(t\right)$ denotes the bias adjusted timeseries of precipitation for hindcast or projections, respectively.

Equation (2) varies with time and does not specify any probability model as the argument of $\mathcal{T}$. In the application of the methodology to the Guadalfeo basin, a NS gamma distribution is employed to characterize the statistical properties of observed, hindcast, and projected data, as detailed by Cobos et al.[82,90]. The probability density function of this distribution is given by:

$$f\left(y(t),\ t;\alpha\right)=\frac{y\left(t\right)^{\alpha\left(t\right)-1}e^{-y(t)}}{\Gamma\ \left(\alpha\ \left(t\right)\right)}\ \text{for}\ y\left(t\right)>0 \tag{4}$$

where $\alpha\ \left(t\right)>0$, Γ denotes the gamma function and $y\left(t\right)$ is the rescaled $x\left(t\right)$ time series:

$$y\left(t\right)=\frac{x\left(t\right)-\mu\ \left(t\right)}{\sigma\ \left(t\right)} \tag{5}$$

In Eqs. (4) and (5), μ and σ are the location and scale parameters that are time-dependent functions, found as the best approach function within a subspace spanned by the set of trigonometric functions (generalized Fourier expansion). This choice allows for obtaining the best fits for all ranges of precipitation values at any time of the year. It is important to highlight that the parameter $\mu\ \left(t\right)$ coincides with $x_o^*\left(t\right)$ for observations and with $x_h^*\left(t\right)$

for hindcast and projected values. This analytical approach effectively captures the pronounced seasonal climate variability prevalent in this semi-arid Mediterranean basin.

Figure 4 shows the NS distribution functions for observed and hindcast data above x_o^* and x_h^*, respectively, of the KNMI_ICHEC-EC-EARTH model at station #112 with the purpose of emphasizing the impact of the proposed NS approach on bias adjustment throughout the year. To elucidate the methodology, two distinct days in January (point P1) and July (point P2) are selected where the inverse values of the distribution functions are both equal to 8 mm. A stationary correction would assign the same percentile to both values, resulting in the same correction for the corresponding projections. The NS hindcast distribution at P1 is close to the 50th percentile, corresponding to 5 mm in the NS distribution of the observed data (P1'). Consequently, the projected value $x_p(t)$ will decrease by 3 mm after the correction. At P2, the percentile of the hindcast distribution is close to 25th, corresponding to almost negligible precipitation for the NS distribution of observations. In this last case, the projected value would decrease by approximately 8 mm. Another example highlighting significant differences throughout the year shows the 95th percentile by the end of the months of February and September, P3 and P4, respectively. The correction for the former entails a reduction of 20 mm (P3'), while for the latter, it implies an increase of approximately 5 mm (P4').

Assessment of bias performance

The validation of the proposed approach is conducted by comparison between the results of several diagnostic parameters after the QDM and NS corrections. The choice of QDM is due to its effectiveness in correction, as noted by Tong et al.[91], compared to other models. The computations were done using the Python CMethods[92] and Marinetools.temporal[90].

The diagnostic parameters employs the monthly-averaged relative bias Δ[93], defined as:

$$\Delta\zeta = \frac{(\zeta - \zeta_r)}{\zeta_r} \cdot 100 \tag{6}$$

where ζ is one of the following parameters: (i) the average number of wet days per month $(\mathrm{n_w})$, (ii) the average precipitation per month $(\mathrm{x_m})$, (iii) the averaged 95th percentile value per month (x_{95})[35,51,58,94], and (iv) the averaged accumulated precipitation per month $(\mathrm{x_{cum}})$; and ζ_r is the corresponding value for the reference data. The observations time series will be the reference data for comparison during the past period.

An indicator based on the root-mean-square-error for percentile q, $RMSE(q)$ is defined as follows:

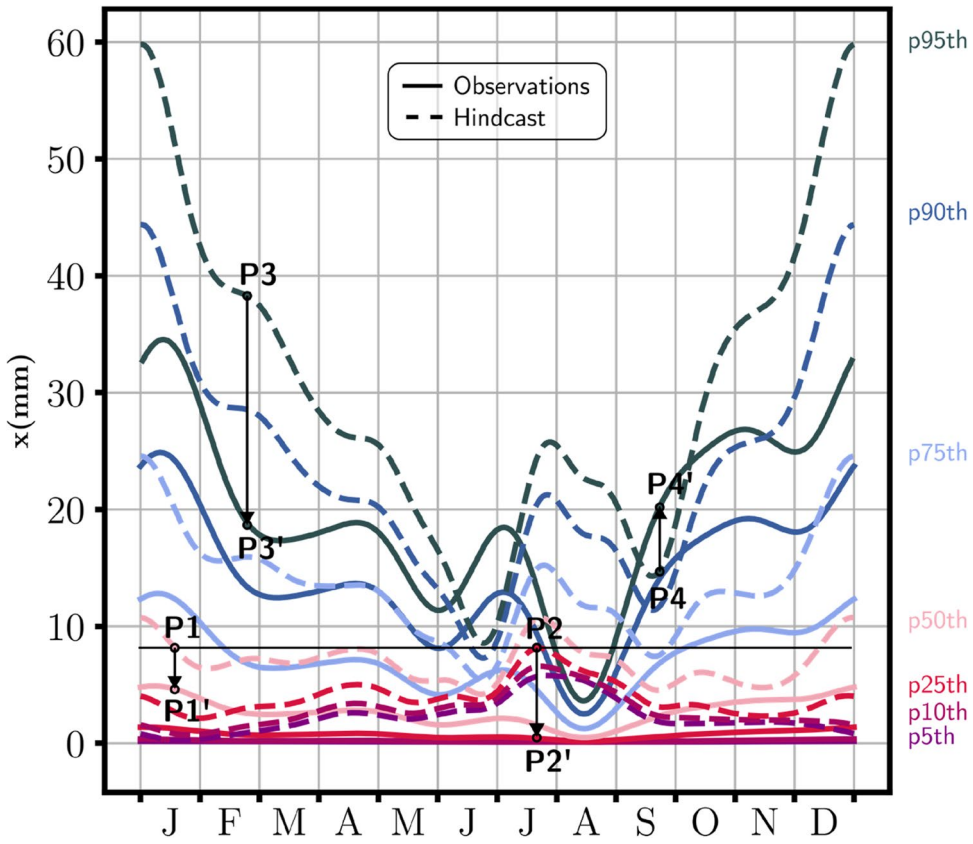

Fig. 4. Non-stationary distribution function of hindcast data above x_h^* (dashed lines) and observations above x_o^* (solid lines) for KNMI_ICHEC-EC-EARTH at station #112. P1 - P4 and P1' – P4' illustrate examples of variability for daily precipitation during the year and bias between observations and hindcast as well.

$$RMSE\,(q)\;=\;\sqrt{\frac{1}{n}\sum\nolimits_{i=1}^{n}\left(\widehat{F_h^{-1}}(q,\,t_i)-\widehat{F_0^{-1}}(q,\,t_i)\right)^2} \tag{7}$$

where $n=365$ days, q is the percentile (usually chosen as 5%, 25%, 50%, 75%, 95%, 99%) and t_i denotes day i of the year. $\widehat{F_0}(q,\,t)$ and $\widehat{F_h}(q,\,t)$ represent the empirical NS distribution functions obtained from a 14-day moving window over the observations and hindcast series, respectively, after the correction with NS and QDM methods. This indicator complements the previous ones as it describes the quality of the correction in probabilistic terms. For a specific percentile, q, $RMSE\,(q)=0$, corresponds to an ideal prefect match between observations and corrections, while positive values indicate differences from the observations.

Finally, the comparison for projections is between ensemble models after the NS and QDM correction. It was conducted by repetition of the methodology for the combination of seven GCM-RCMs. After that, it was assessed the multi-model uncertainty through the average of all models.

Results

In this section, the results of applying the occurrence and magnitude adjustment proposed to hindcast and projected timeseries are presented. Firstly, the NS non-exceedance probability of x_o^* and the corresponding threshold obtained for adjustment are depicted for all the GCM-RCMs considered. In addition, with the aim of showing the performance of the methodology on individual models, the analysis focus on the DMI-ICHEC-EC-EARTH model. More precisely, the transfer function, $\mathcal{T}$, between the hindcast and observations of that model is illustrated. Subsequently, the proposed development indicators are assessed on a monthly scale for both the QDM and the proposed method for the selected model. It is important to remark that QDM results do not consider the interannual variability in its formulation, even though they are represented in the same way as NS results for comparison. The section concludes with the presentation of the multi-model ensemble behaviour of the two methods for all GCM-RCM models considered and two stations at low and high altitude and assessing the future impact on Guadalfeo river basin. In the Supplementary Material can be found the results for the remaining GCM-RCM models shown in Table 2.

Non-stationary occurrence bias-adjustment

Figure 5 displays the probability that does not rain, e.g., $x \leq x_o^*$, obtained for hindcast data of seven GCM-RCM models and of observations, at the stations of the Guadalfeo river basin.

Observations exhibit a pronounced seasonal variation in the number of days without precipitation, with a clear peak during spring and summer, reaching nearly 95% in July and August, and maintaining relatively constant values during other seasons. Overall, there is approximately a 30% difference in the number of non-rainy days between the drier days and the wet period. The minimum number of observed non-rainy days out of summer season corresponds to ~40% at stations #112, #601 and #801, while the maximum values (>80%) are observed at stations #116, #176 and #85. The hindcast data also reflects this pattern albeit less prominently at stations #93 and #801 associated to the fact that those results come from grid points located at mountainous environments. Generally, both drizzle and drier effects are evident for hindcast time series at all the stations considered, except for #93 where only a drizzle effect is present throughout the year for all models. All the models underestimate the probability of not exceeding x_o^*. This is especially true during the winter months for all the seasons considered. At the lower altitude stations, the models fit the observed summer data better. At the higher altitude stations (#93, #801), the models underestimate the non-exceedance probability and do not adequately represent the seasonality, except for station #112. The KNMI-ICHEC-EC-EARTH model underestimates the threshold in a generalized manner across all the stations considered.

Figure 6 shows the NS thresholds obtained with Eq. (1) for the hindcast data. The vertical axis is presented in a logarithmic scale to better discern the differences of up to two orders of magnitude in the variable $x_h^*(t)$ throughout the year. A pronounced temporal variability in x_h^* is evident, with values exceeding 10 mm at stations #93 and #801. As previously articulated, a pervasive drizzle effect is noted across all models and seasons within the Guadalfeo river basin, where x_h^* remains above 0.1 mm. At station #601, in all models, except KNMI_ICHEC-EC_EARTH, x_h^* presents values below 0.8 mm. Notably, at this station, models such as DMI_ICHEC-EC-EARTH, DMI_NCC_NorESM1-M, SMHI_IPSL_IPSL-CM5A-MR, and SMHI_NCC-NorEMS1-M depict prolonged periods of drier effect. In contrast, at station #93, the mean threshold value stands at approximately 4 mm, signifying a substantial deviation from the reference value (x_o^*).

Figure 7 depicts the relative bias, $\Delta\, n_w$, of the monthly number of rainy days in the hindcast data with respect to the observations and the corresponding corrected series for DMI_ICHEC-EC-EARTH model. The colour gradient is divided into three parts: values with a strong negative difference lower than −100% are in purple, values between −100% and 100% are in a colour red-white-blue gradient and finally, values higher that 100% that presents a significant positive difference are in dark green. Reds and blues highlight periods of drier and drizzle effects, respectively. In general, the hindcast produces more rainy days at all basin stations with differences that rise to almost 800% at station #176. The exception is the station #601, where the count is lower in almost the entire year. At stations #85, #100, #112, and #601, there are less rainy days in June. Station #93 shows a mean overestimation of 175% compared to the observation series for the same period. The NS approach significantly reduces the number of rainy days at all stations where it generally remains below ±10%, except for the dry season where differences reach up to ±40% approximately. It is noticeable that the largest variations with respect to the observation series occur in summer, primarily in July and August. The model KNMI_ICHEC-EC-EARTH overestimates the number of rainy days at station #116 and July a 3817% (Fig. S01-01 of SM) and the correction reduced that value to 150%. During this period, the limited number of observed rainy days (around

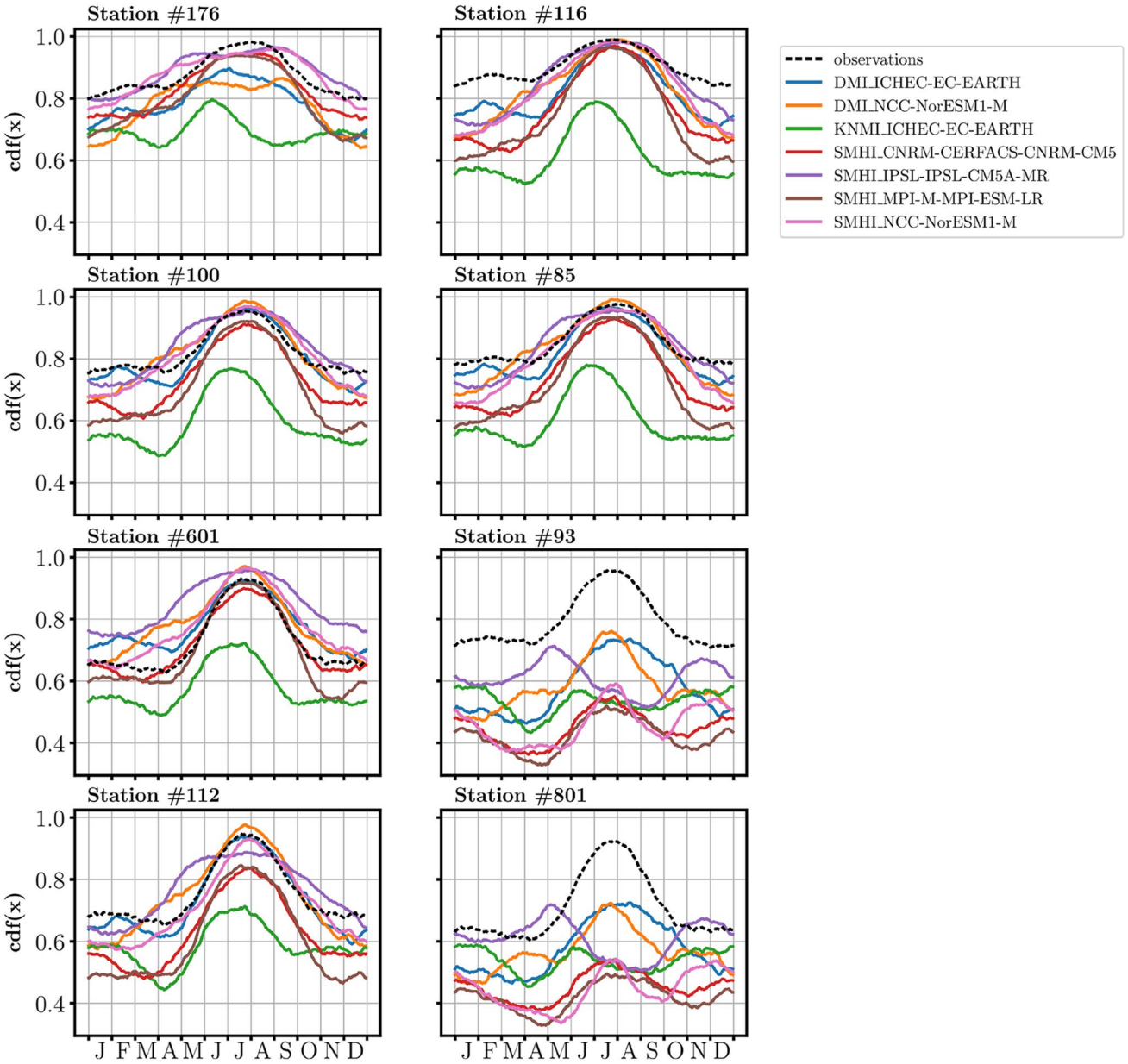

Fig. 5. Empirical non-exceedance probability of x_o^* of seven hindcast models $\left(\widehat{F}_h\left(x_o^*\right)\right)$ and of observations $\left(\widehat{F}_o\left(x_o^*\right)\right)$ at the stations of the Guadalfeo river basin.

one day per month on average) poses challenges for correction. Nevertheless, it is important to highlight the effectiveness of the method.

Non-stationary intensity bias-adjustment

Figure 8 depicts the transfer function, $\mathcal{T}\left(F_p\left(x_p\left(t\right);t\right)\right)$ between the hindcast data and observations across all stations considered within the basin. The computation of $\mathcal{T}$ was done over the year for probability values $F_p\left(x_p\left(t\right);t\right)$ ranging from 0.001 to 0.999 (y-axis). In general, for probabilities below 0.8, $\mathcal{T}$ exhibits fluctuations within the range of -10 to 10 mm. Notably, the station at the highest altitude, #801, consistently registers a negative value, and station #93 even presents differences extending up to -50 mm. This phenomenon is attributed to the significant disparities observed between all models and the observations at the corresponding station, as outlined in Sect. 4.1. Above that probability value, the behaviour of each station diverges. Stations #176 and #100 manifest a temporal variability characterized by positive corrections in winter and autumn, and negative corrections in summer. Similarly, stations #116 and #85 display positive corrections in spring. Conversely, stations #93 and #801 implement corrections by diminishing precipitation throughout the year, reaching minimal values during the summer months for the remaining models (see also Figs. S02-01 to S02-07 of SM).

Figure 9 illustrates the bias performance by showing the relative bias with respect to observations (taken as reference data in Eq. 6) of hindcast data (left panels), data after the QDM adjustment (mid panels) and after the

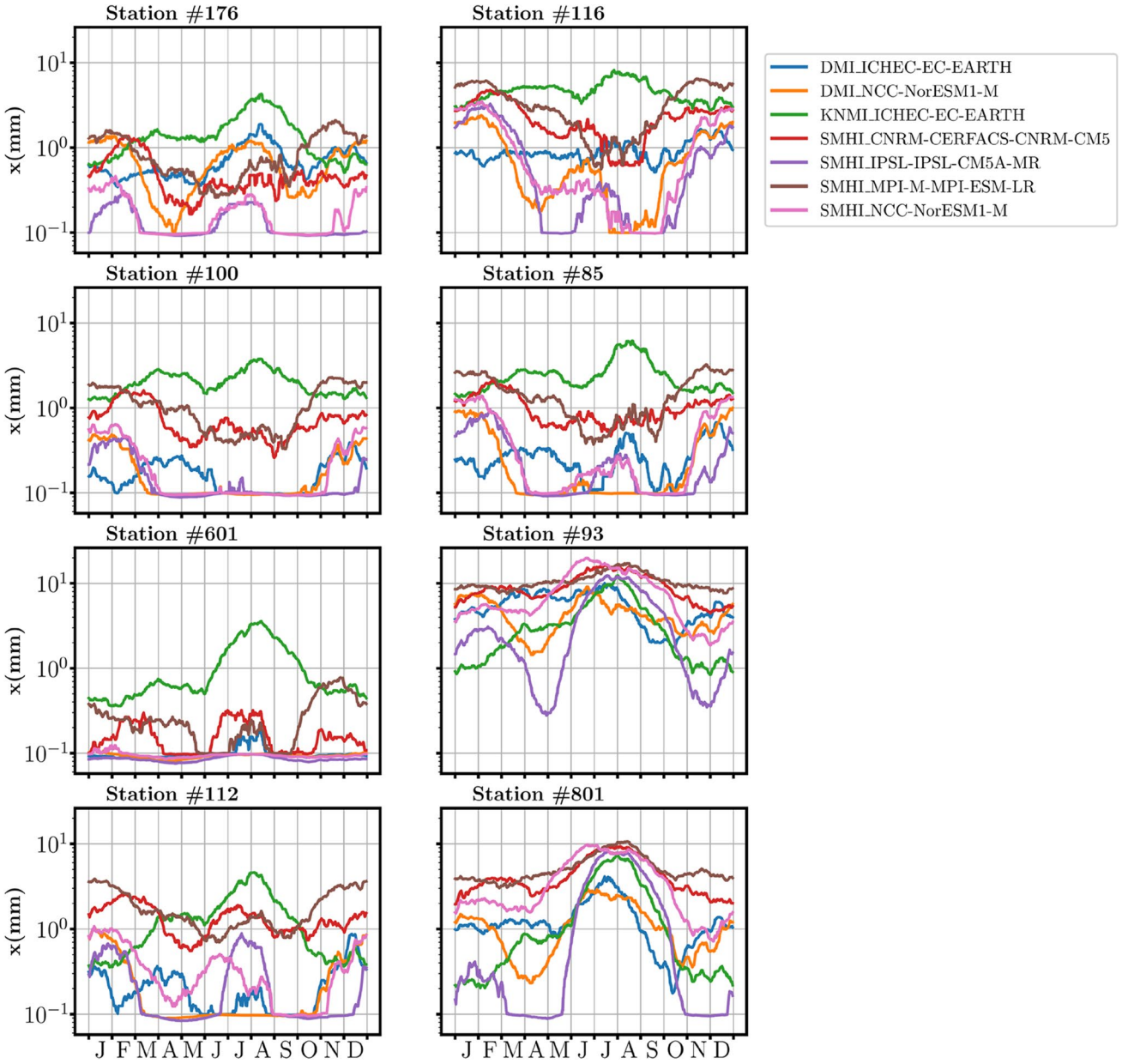

Fig. 6. Non-stationary obtained thresholds $\left(x_h^*(t)\right)$ for all models considered at stations in the Guadalfeo river basin.

NS adjustment (right panels) for the following descriptors (from top to bottom rows): the mean precipitation per month, ($\mathrm{x_m}$), the monthly averaged accumulated precipitation, ($\mathrm{x_{cum}}$) and the averaged 95th percentile event per month (x_{95}).

The hindcast shows a significant reduction in comparison to observations for all the descriptors throughout the year for stations #176, #116, #100 and #85 that are located at low altitudes and an increase for the mountainous stations (#93, #112, #801), except for July and August, the drier months. A transitional behaviour can be observed at station #601 located at an intermediate altitude. For the relative bias on monthly mean ($\Delta\, x_{\mathrm{m}}$), the highest reductions are found, ranging, in general, from 50 to 75% for stations #176, #116 and #85 and with lower values for station #100. In August, the hindcast data even show a significant increase close to 116% for station #100. Station #100 also exhibits a significant reduction, albeit with the caveat of overestimating the average precipitation in August by more than twice the observed value. At the remaining stations (#112, #93, #601, and #801) there is an increase in the average precipitation (depicted in blue). The largest differences are found in July or August except for #93 in which hindcast divergence with observations are obtained in spring months. After the application of the QDM adjustment, the variation between hindcast and observations is notably diminished except in August when a significant overestimation is noted for all stations. The average precipitation may be higher or lower than the observed values depending on the station and month. In stations #176 and #806, the hindcast yields an average precipitation more than five and four times higher, respectively,

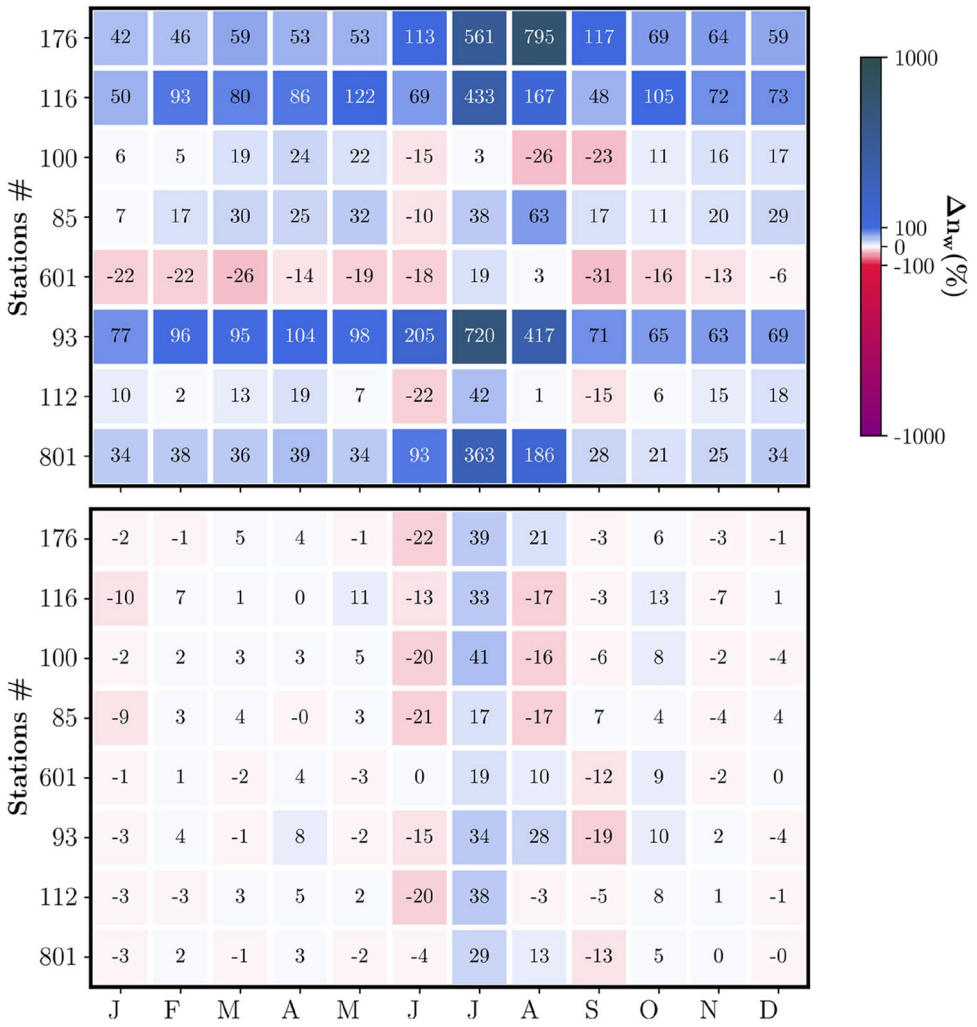

Fig. 7. Percentage of the monthly relative difference of the number of rainy days, $\Delta\, n_w$, of observations and hindcast data (upper panel) and observations and the corresponding corrected series (lower panel) for DMI_ICHEC-EC-EARTH model. Colour scale of indicator is established jointly with Fig. 9.

than the observations. Finally, the NS approach improves the adjustment, restricting the average precipitation within ± 10% for all the stations except for #601 along the year apart from the months of July and August where a general underestimation of up to 60% persists.

The relative bias on cumulative average precipitation ($\Delta\, x_{\mathrm{cum}}$) follows a similar pattern with the larger values found on the dry months where hindcast relative bias reach values close to 1000% higher at stations #176, #93 and #801. QDM adjustment reduces differences for the wetter months but increase them for July and August for stations at the lower altitudes (#176, #116, #100, #85 and #601). The proposed NS method works in general much better than QDM throughout the year for all the stations except for #601 that shows larger absolute values for the wet months. The relative bias is smaller than 25% and very often close to 10% for all the non-dry months. In July and August, the performance of this method is better than QDM although it still fails to reproduce the behaviour at stations at the lower (station #176) and higher (station #801) altitudes. This may be due to the scarcity of precipitation data of observations during those months that is responsible for more uncertain estimations of the distribution function. It is worth noting how the NS method significantly improves the summer bias, much better than QDM, for those GCM-RCM models that exhibit a significant bias (Fig. S03-01, 03, 04 of SM).

The QDM effectively reduces this relative bias on $\Delta\, x_{95}$ across all stations throughout the year with values close and sometimes smaller in absolute value to those obtained with the NS method. The months of July and August prove to be challenging to adjust, particularly with the QDM approach for which relative differences close to 1000% are even obtained at station #176 likely due to that method does not consider the temporal variability of precipitation. The NS adjustment gives, generally, smaller values during the dry months ranging from negligible differences at station #93 to a value close to 210% at #176.

The NS correction reduces bias on the diagnostic parameters in 7 to 9 out of the 12 months of the year in comparison to QDM for five of the stations (#176, #116, #100, #93, #801). Three stations (e.g., #601, #112, or #85), located in areas with more complex orography, show improvement with the NS method in 3 to 5 months. Overall, in the study area, the months that show better correction cover the spring-summer season (March

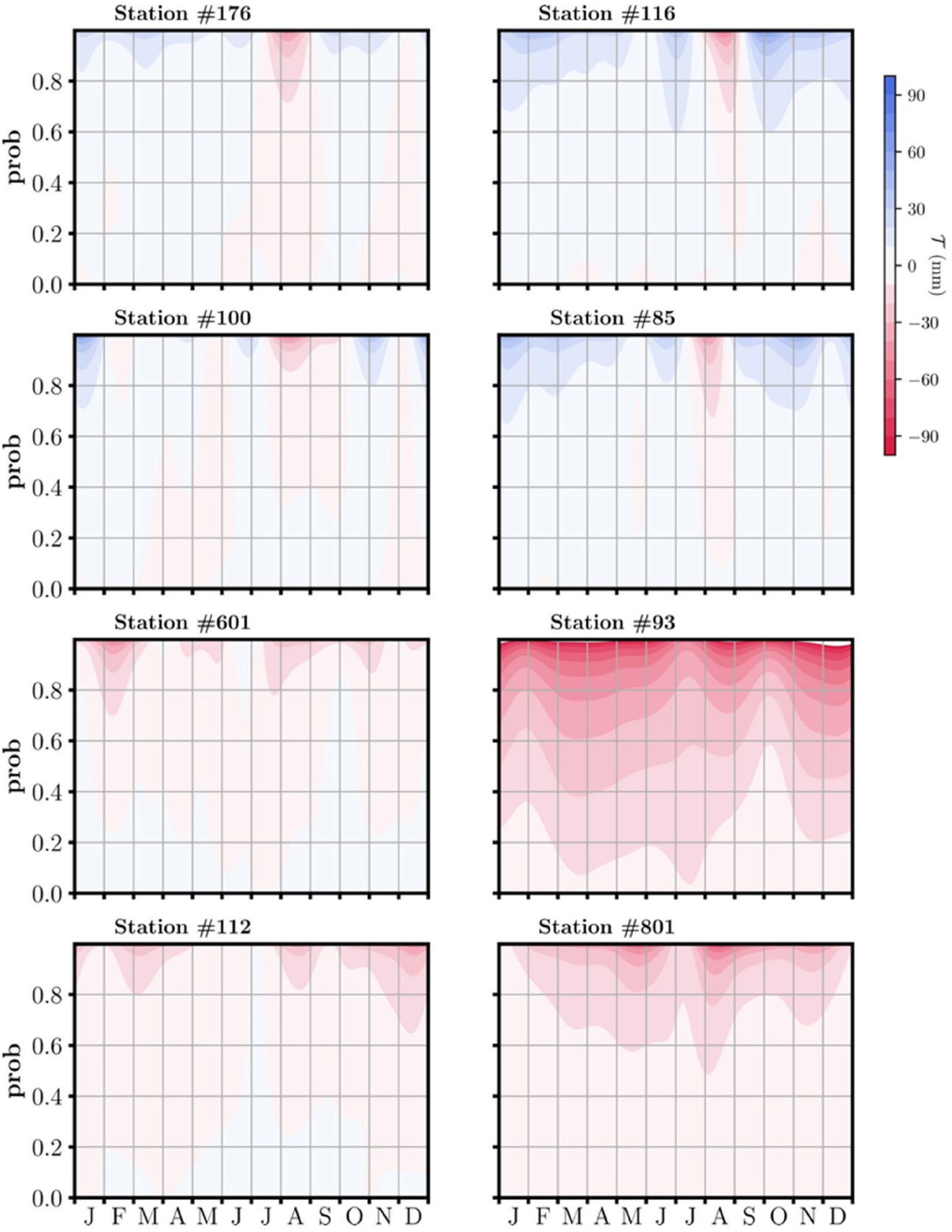

Fig. 8. Transfer functions $\mathcal{T}$ (Eq. 3) of DMI-ICHEC-EC-EARTH model and observations for stations at Guadalfeo river basin.

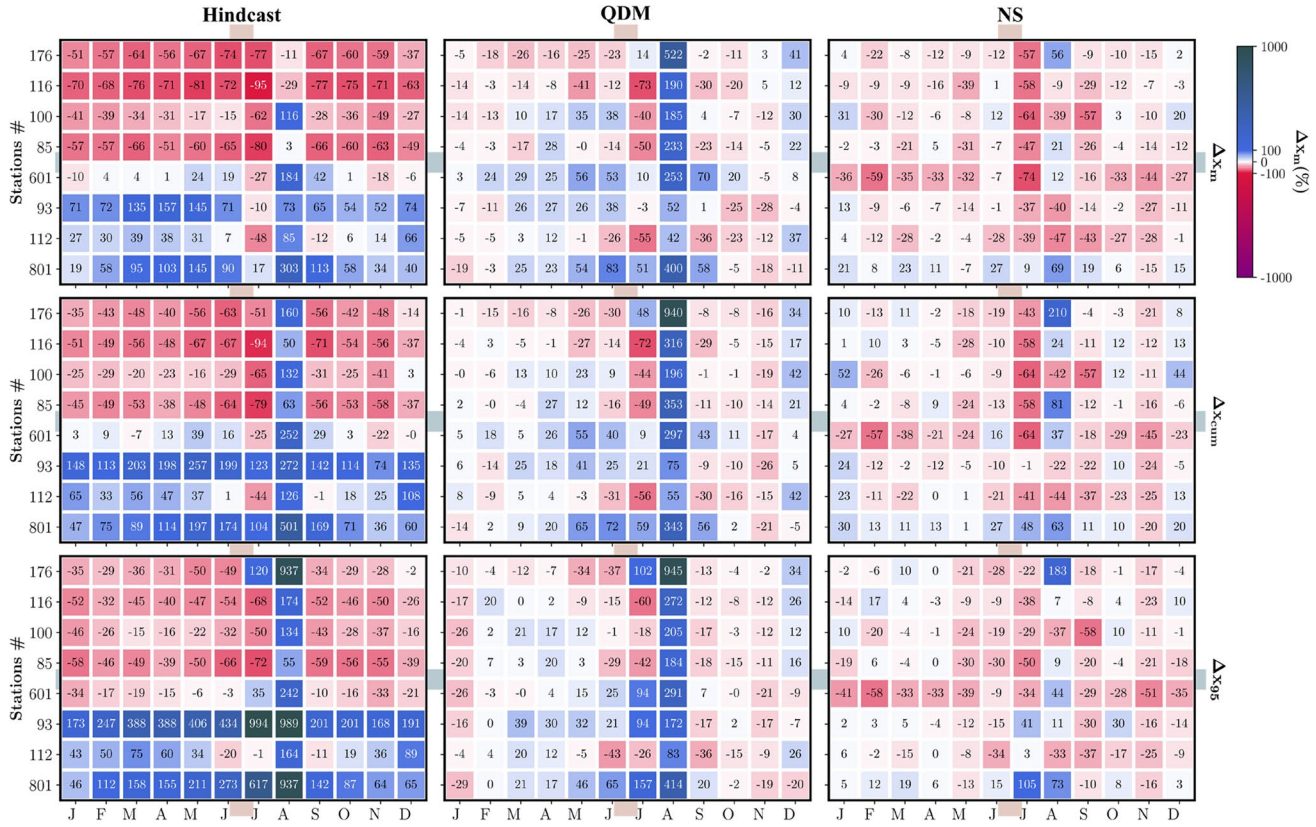

Fig. 9. Relative bias of hindcast data (left panels), QDM adjusted data (mid panels), and data adjusted with the NS proposed method (right panels), for DMI-ICHEC-EC-EARTH model using observations as reference data. Rows from top to bottom depict Δx_{m}, Δx_{cum} and Δx_{95}, respectively.

Station #	Percentile					
	5	25	50	75	95	99
176	0.36 ± 0.04 0.29 ± 0.03	0.19 ± 0.02 0.70 ± 0.07	0.89 ± 0.09 1.21 ± 0.12	1.71 ± 0.18 1.68 ± 0.17	3.50 ± 0.36 4.57 ± 0.47	12.30 ± 1.26 13.91 ± 1.43
116	0.58 ± 0.06 0.76 ± 0.08	0.53 ± 0.05 1.06 ± 0.11	1.59 ± 0.16 1.84 ± 0.19	2.54 ± 0.26 2.01 ± 0.21	5.88 ± 0.60 4.99 ± 0.51	18.40 ± 1.89 12.21 ± 1.25
100	0.14 ± 0.01 0.05 ± 0.01	0.18 ± 0.02 0.24 ± 0.02	0.77 ± 0.08 1.30 ± 0.13	1.83 ± 0.19 4.09 ± 0.42	5.80 ± 0.60 16.61 ± 1.71	16.21 ± 1.67 33.99 ± 3.49
85	0.55 ± 0.06 0.33 ± 0.03	0.23 ± 0.02 0.67 ± 0.07	1.42 ± 0.15 1.34 ± 0.14	3.30 ± 0.34 2.60 ± 0.27	6.46 ± 0.66 7.27 ± 0.75	16.27 ± 1.67 16.04 ± 1.65
601	0.27 ± 0.03 0.03 ± 0.00	0.10 ± 0.01 0.21 ± 0.02	0.85 ± 0.09 0.62 ± 0.06	3.00 ± 0.31 2.05 ± 0.21	7.34 ± 0.75 9.24 ± 0.95	11.81 ± 1.21 20.10 ± 2.07
93	0.09 ± 0.01 0.30 ± 0.03	0.29 ± 0.03 0.54 ± 0.06	0.71 ± 0.07 1.07 ± 0.11	1.45 ± 0.15 2.43 ± 0.25	5.63 ± 0.58 10.71 ± 1.1	8.97 ± 0.92 21.21 ± 2.18
112	0.21 ± 0.02 0.15 ± 0.02	0.14 ± 0.01 0.2 ± 0.02	0.53 ± 0.05 0.56 ± 0.06	1.30 ± 0.13 1.61 ± 0.17	4.19 ± 0.43 7.78 ± 0.80	9.51 ± 0.98 19.37 ± 1.99
801	0.07 ± 0.01 0.16 ± 0.02	0.15 ± 0.01 0.30 ± 0.03	0.42 ± 0.04 0.99 ± 0.10	1.35 ± 0.14 3.14 ± 0.32	4.60 ± 0.47 13.27 ± 1.36	10.92 ± 1.12 28.91 ± 2.97

Table 3. Comparison of performance between NS and QDM using RMSE(q) (eq. 7) and their 95% confidence intervals for the percentiles q corresponding to 5, 25, 50, 75, 95 and 99 for DMI-ICHEC-EC-EARTH model. In each cell, on top is the value obtained with the NS approach while bottom one corresponds to the QDM method.

to August) and part of winter (December to January). The diagnostic parameter Δx_{95}, which shows a better correction by NS during the spring-summer months, does not experience significant improvement compared to QDM during the autumn-winter months (September to February).

The differences in the performance of both approaches can also be assessed in Table 3 that shows, for all the meteorological stations, the values of $RMSE\,(q)$ and their 95% confidence intervals for six different percentiles

corresponding to values of q ranging from 5 to 99. In each cell, on top is the value obtained with the NS approach while the bottom one corresponds to the QDM method. The performance of both approaches is better for the smaller percentiles. Taking the 50th percentile as a reference, it can be observed that the NS method shows an RMSE below 1 mm for all stations except #116 and #85. The average RMSE value for the 50th percentile across all stations is 0.88 mm for NS while the value rises slightly 1 mm (1.12 mm) for QDM. For most of the stations and percentiles the error is smaller for the NS approach, with values that get to double (stations #100, #601, #93, #112 for the 99th percentile and station # 93 for the 95th percentile) and are close to triple (station #801 for the 99th percentile and stations # 100 and #801 for the 95th percentile).

As the RCMs inherit the biases from the GCM output, it is important to combine different GCM-RCMs models to reduce the uncertainty of the estimated impacts[56]. Figure 10 depicts the monthly ensemble mean values of the number of rainy days, average monthly precipitation cumulative average and 95th percentile precipitation from all GCM-RCMs following the QDM and NS adjustments for the station #176 (near the coast < 50 m a.s.l) and station #93 (> 1000 m a.s.l). The figure also includes the minimum and maximum values to show the variability between individual model values. To assess the impact on the future, the value obtained from the observed series has also been added as a reference (solid horizontal black line for each month). The ensemble averages of all the parameters are, in general, closer to the observations with the NS correction than with the QDM bias adjustment. For this last methodology, there is a larger variability between the values of the individual models than for the NS approach that reduces the differences between them and, therefore, the uncertainty associated to the parameters. Both methods have a similar performance at both stations for the number of rainy days, with values that differ about 1 day between models for the NS method and that are closer to or exceed 2 days for QDM in April-May and October-November, that are transitions months between the dry and wet seasons. For x_{m}, the largest variability between models is found for QDM approach that is close to 10 in the dry season at station #93 and to 11 in August for station #176. The QDM technique gives, in general, greater mean ensemble values than observations except for the months between October and January, while the NS gives similar ensemble values. Again, the variability between the values projected by individual climate models is greater for QDM that even doubles the differences of the NS (values in January closer to 82 mm for the former one and to 40 for the last approach). The monthly cumulative values x_{cum} show less variability than projected models during the dry season, which is also reduced when the NS bias adjustment is applied. The values of x_{95} are also closer to observations for NS than for QDM bias adjustment. QDM predicts larger ensemble values except for October-December at #93 and gives similar values at station #176. The variability between models is close to 5 mm for NS and doubles for QDM that even reaches 18 mm in January for station #93.

Figure S05-01 (SM) shows the monthly variation of ensemble indicators for the GCM-RCM model from Table 2. It is worth noting that, although uncertainty is reduced with the use of the NS model, the temporal variability of precipitation at some stations still exhibits differences between the minimum and maximum values, which in some cases exceed 10 mm (see the variable x_m for station #116 in July or x_{95} for station #85 in January). This indicates high variability among climate models.

Discussion

The bias adjustment methodologies correct the large disparity of the distribution of GCM-RCMs products. The adjustment of phenomena that are not always active such as the precipitation requires to set up a minimum threshold to obtain the same proportion of observations and hindcast data. In this approach, a time varying threshold is adopted to guarantee that the correction gives the same proportion of observed and hindcast data. The methodology proposed by Vrac et al.[29] was successfully extended to the NS case during drier days while a modified version of the threshold adaptation method of Schmidli et al.[35] is adopted for wetter days. The proposed methodology results in a NS threshold. The key role played by the NS character of the method in adjusting the precipitation bias is shown in Fig. 4. Furthermore, although the presented methodology has been applied to precipitation due to the challenges posed by its high seasonality and intermittency in semi-arid basins, it can also be successfully applied to other variables. In other variables, the correction of the occurrence will be unnecessary.

In the application proposed, the year has been taken as the base period, using a Gamma NS theoretical probability model (Eqs. 4 and 5) for the adjustment of the intensity of daily precipitation. The NS threshold (x_h^*) was selected as the location parameter of Gamma distribution obtained in the first step in the methodology, contributing to the robustness of the approach. The use of the year as the time interval, I, for the analysis allows to capture the seasonal variation and its choice is conditioned by the length of the available historical period of 35 years. Larger temporal scales can also be considered by using several years as in Cobos et al.[82] when available historical data are long enough. While in this study, a single distribution function successfully represents the NS behaviour of precipitation, the methodology can also be applied to piecewise distributions as showed in Cobos et al.[82] if there is a need to use different distributions for the tails and the central body. In those cases, it is also possible to establish a link between the NS threshold and the parameters of the distribution. It must be noted that the methodology (a) does not prescribe any kind of theoretical probability model, (b) does not correct independently the extreme events, (c) does not require any kind of extrapolation method to correct the projected extremes beyond the observed maxima and (d) removes the bias at different time scales (from days to decades).

The proposed methodology accounts for the temporal dependency of data by means of a time dependent parametrization of the NS probability distributions. The probability distributions are created by splitting the time series in interval of one year. The empirical distribution is generated with a moving window which size is related to physical mechanisms, e.g., in the case of precipitation is related to the minimum period that define the motion of low pressures fields which is around 14 days at the Mediterranean basin. Furthermore, it must be required a minimum size of the dataset to create realistic empirical cumulative distributions for the correction of occurrence and to fit the theoretical distributions.

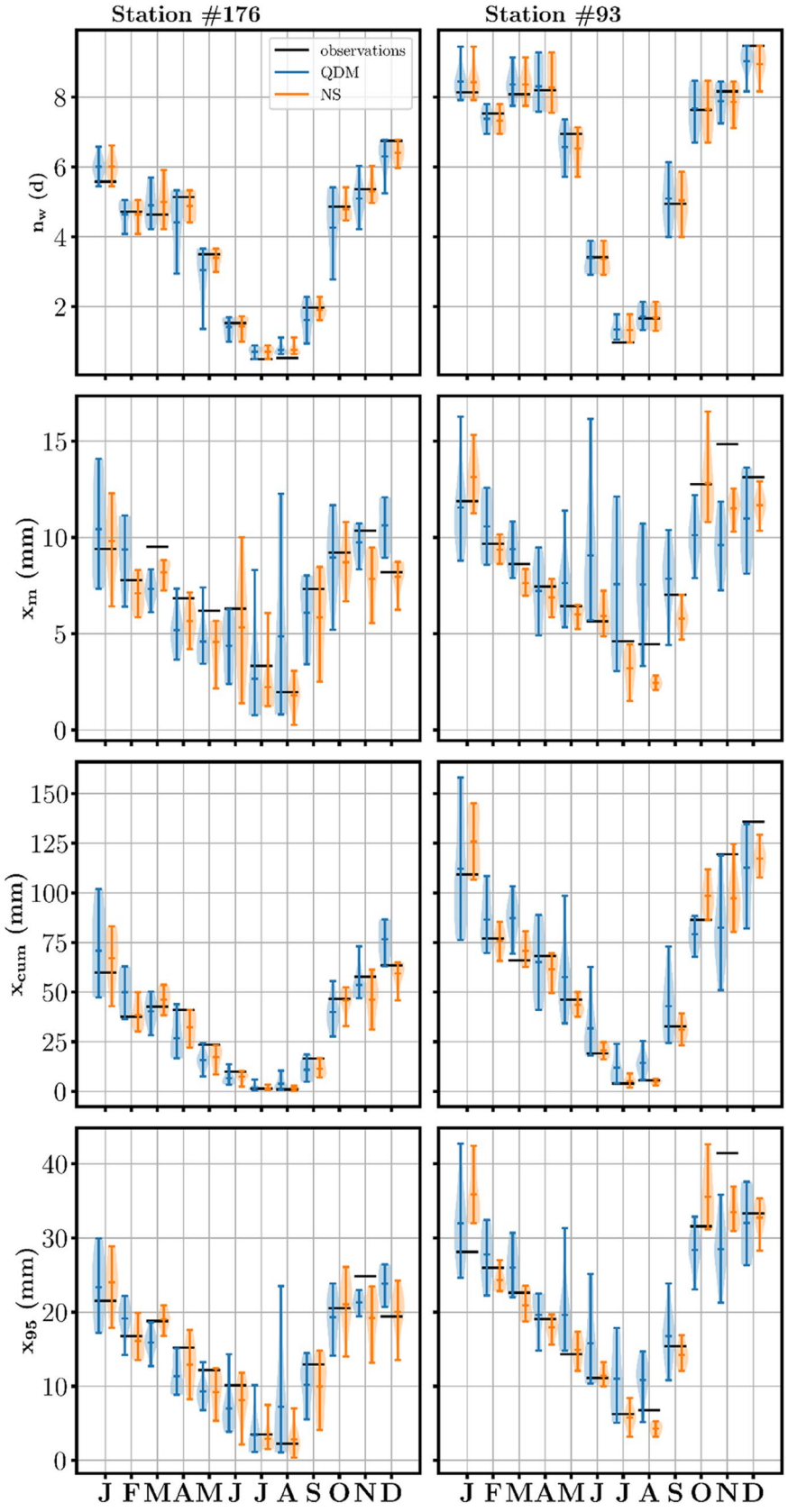

Fig. 10. Plot of the monthly variation of n_w, x_m, $x_{95}$and x_{cum} of the ensemble of the models (minimum, mean and maximum values) for projections after the QDM and NS bias adjustment at two representative stations of the study area. Solid horizontal black lines stand for the observations (1970–2005).

Monthly averaged values of four indicators were evaluated in the present study as it is usual in the existing literature, but any longer or shorter periods can be used for validation purposes. The results show that the proposed bias-correction method is remarkably effective in reducing the model bias. So far, it has only been applied in a univariate framework (i.e., one location and one variable at a time), however, it would be interesting to extend the NS approach to a multivariate context following the suggestions on previous studies[38,95,96].

The sensitivity of modeling uncertainty with altitude is significant as in other studies[97–99] (and references herein). In general, the studied GCM-RCM models overestimate the frequency of precipitation in high mountain areas (cells A, B, C in Fig. 1) from observations at nearby stations (#93, #112, #801). An anomalous effect is observed at station #601, located in a valley between the confluences of Sierra Nevada and Sierra de la Contraviesa, where the models analysed, from results at cell G, underestimate the number of events per year and the amount of precipitation. These differences could highlight the limitations of regionalized GCM-RCMs to reproduce precipitation dynamics in complex topographies although, in this case, it could also be related to an overextension of the semi-arid climate conditions of Almeria, located to the East. Although this aspect does not limit the application of the proposed bias adjustment method, it could become a limitation for the joint adjustment on multiple locations. Projections show a slightly decrease in the number of wet days throughout the year, particularly in April, October, and December. Regarding the amount of precipitation, more severe and delayed drier seasons are expected in the future under the RCP 8.5. Those results confirm the so-called Indian Summer, already reported by Rizou et al.[100], among others, and observed in Lira-Loarca et al.[101] for wave climate. The NS adjustment also reflects a potential increase in the magnitude of extreme events during the summer and winter, primarily for stations located near the coast. The ensemble of seven models reduce the variability of the mean along the year.

The similarity between $\Delta\,\mathbf{x}_{95}$ and $\Delta\,\mathbf{x}_{\mathbf{cum}}$ may be attributed to the precipitation patterns (short and intense) in the Mediterranean basins of Andalusia. The region experiences low precipitation, characterized by short-duration events. The reduction of the ensemble bias allows us to observe that, according to the NS adjustment results in the Guadalfeo River basin, the main reduction in mean precipitation occurs during the spring, summer, and autumn seasons in the upper part of the basin, while an increase is observed in winter (station #93). Comparable results are in Zayandeh-rud basin[102]. However, when it does rain, it tends to be intense, establishing a connection between $\mathbf{x}_{95}$ and $\mathbf{x}_{\mathbf{cum}}$. In Mediterranean regions and similar areas worldwide, models yield a higher number of rainy days in mountainous areas and significantly greater precipitation compared to observed data. If these models are employed to input hydrological models without appropriate correction, not only for precipitation but also for other climate variables such as temperature or solar radiation, it will result in soil moisture conditions conducive to surface runoff. Those differences would also highly alter the pluvio-nival models at Sierra Nevada basin, predicting much more snow during winter than it is commonly observed. Additionally, hydrological models that considers snowmelt contributions will carry much more water along the river during spring. The unbiased projections will serve as a valuable source of information that will benefit the impact assessment of climate change precipitation properties, which are crucial to assess the hydrological response of semi-arid mountainous regions all over the world.

Conclusions

A bias adjustment model based on non-stationary probability distributions was proposed and successfully applied to the precipitation on a semi-arid basin. The bias adjustment of the precipitation was a challenge due to its high seasonality and intermittent behaviour. In our research, all the indicators used to measure its performance experience a reduction of the bias after its application. Regardless of the station location, the effect of drizzle and drier conditions is satisfactorily corrected, overall achieving a bounded relative bias of the number of wet days around $\pm 5\%$ throughout the year. The occurrence correction reduced the monthly difference observed between the hindcast and observed data in comparison to the QDM method. In some cases, the relative reduction reaches 800%, getting differences with observations lower than one day. The temporal patterns of the corrected precipitation strongly differ between GCM-RCM models. The proposed method shows an appropriate behaviour under such conditions, consistently reducing variability among models in all cases. The sensitivity of the model's uncertainty in regions with a high altitudinal gradient is also significantly reduced with the NS approach. Overall, GCM-RCM's models consistently underestimate the mean precipitation by a relative value close to 57% on average for low altitudes (station #176) and overestimate by about 93% for high altitudes (station #801). The bias of the ensemble of projections after the NS correction shows bounds that again are lower than one day, ± 3 mm, ± 6 mm and ± 20 mm for the average number of wet days per month, the average precipitation per month, the averaged 95th percentile value per month, and the average accumulated precipitation per month, respectively. The method reduces it performance on root mean square error from the smaller to higher percentiles. In those stations located at higher latitudes, the error on percentiles 95 and 99 of QDM double or triple the error obtained with NS. The NS method maintains the annual pattern of precipitation on ensemble projections of observed data and overcomes the non-stationary-related limitations which significantly reduces the large uncertainty in the precipitation.

Data availability

The corrected time series of the climate models employed, the RCP8.5 scenario for the Guadalfeo river basin and the non-stationary parameters obtained from the fitting algorithm for all models and stations are accessible on Zenodo (https://doi.org/10.5281/zenodo.13830694).

Received: 20 May 2024; Accepted: 17 October 2024
Published online: 29 October 2024

References

1. Essa, Y. H., Hirschi, M., Thiery, W., El-Kenawy, A. M. & Yang, C. Drought characteristics in Mediterranean under future climate change. *Clim. Atmos. Sci.* **6**(1), 133. https://doi.org/10.1038/s41612-023-00458-4 (2023).
2. Chokkavarapu, N. & Mandla, V. R. Comparative study of GCMs, RCMs, downscaling and hydrological models: a review toward future climate change impact estimation. *SN Appl. Sc* **1**(12), 1698 (2019).
3. Naz, B. S. et al. Regional hydrologic response to climate change in the conterminous United States using high-resolution hydroclimate simulations. *Glob Planet. Change.* **143**, 100–117 (2016).
4. Anav, A. et al. Dynamical downscaling of CMIP6 scenarios with ENEA-REG: an impact-oriented application for the Med-CORDEX region. *Clim. Dyn.* **62**, 3261–3287. https://doi.org/10.1007/s00382-023-07064-3 (2024).
5. Torma, C., Giorgi, F. & Coppola, E. Added value of regional climate modeling over areas characterized by complex terrain-precipitation over the alps. *J. Geoph Res. Atmos.* **120**(9), 3957–3972. https://doi.org/10.1002/2014JD022781 (2015).
6. Buonomo, E., Jones, R., Huntingford, C. & Hannaford, J. On the robustness of changes in extreme precipitation over Europe from two high resolution climate change simulations. *Q. J. R Meteorol. Soc.* **133**(622), 65–81. https://doi.org/10.1002/qj.13 (2007).
7. Giorgi, F. Thirty years of regional climate modeling: where are we and where are we going next?. *J. Geophys. Res. Atmos.* **124**, 5696–5723. https://doi.org/10.1029/2018JD030094 (2019).
8. Jacob, D. et al. An inter-comparison of regional climate models for Europe: model performance in Present-Day climate. *Clim. Change.* **81**(S1), 31–52. https://doi.org/10.1007/s10584-006-9213-4 (2007).
9. Piani, C. et al. Statistical bias correction of global simulated daily precipitation and temperature for the application of hydrological models. *J. Hydrol.* **395**(3), 199–215. https://doi.org/10.1016/j.jhydrol.2010.10.024 (2010).
10. Vidale, P. L., Lüthi, D., Frei, C., Seneviratne, S. I. & Schär, C. Predictability and uncertainty in a regional climate model. *J. Geoph Res.* **108**(D18), 4586. https://doi.org/10.1029/2002JD002810 (2003).
11. Chen, J., Brissette, F. P., Chaumont, D. & Braun, M. Finding appropriate bias correction methods in downscaling precipitation for hydrologic impact studies over North America. *Water Resour. Res.* **49**, 4187–4205 (2013).
12. Kotlarski, S. et al. Regional climate modeling on European scales: a joint standard evaluation of the EURO-CORDEX RCM ensemble. *Geosci. Model. Dev.* **7**(4), 1297–1333. https://doi.org/10.5194/gmd-7-1297-2014 (2014).
13. Li, J., Sharma, A., Evans, J. & Johnson, F. Addressing the mischaracterization of extreme rainfall in regional climate model simulations – A synoptic pattern based bias correction approach. *J. Hydrol.* **556**, 901–912. https://doi.org/10.1016/j.jhydrol.2016.04.070 (2018).
14. Giorgi, F., Raffaele, F. & Coppola, E. The response of precipitation characteristics to global warming from climate projections. *Earth Syst. Dyn.* **10**(1), 73–89. https://doi.org/10.5194/esd-10-73-2019 (2019).
15. Sheffield, J. et al. North American climate in CMIP5 experiments. Part II: evaluation of historical simulations of intraseasonal to decadal variability. *J. Clim.* **26**(23), 9247–9290 (2013).
16. Maurer, E. P. & Pierce, D. W. Bias correction can modify climate model simulated precipitation changes without adverse effect on the ensemble mean. *Hydrol. Earth Sys m Sc.* **18**(3), 915–925. https://doi.org/10.5194/hess-18-915-2014 (2014).
17. Pierce, D. W., Cayan, D. R., Maurer, E. P., Abatzoglou, J. T. & Hegewisch, K. C. Improved Bias correction techniques for Hydrological simulations of Climate Change. *J. Hydrometeorol.* **16**(6), 2421–2442. https://doi.org/10.1175/JHM-D-14-0236.1 (2015).
18. Lucas-Picher, P. et al. Convection-permitting modeling with regional climate models: latest developments and next steps. *Wiley Interdisciplinary Reviews: Clim. Change* **12**(6), e731 (2021).
19. Solman, S. et al. *The future scientific challenges for CORDEX* (2021) https://cordex.org/wp-content/uploads/2021/05/The-future-of-CORDEX-MAY-17-2021.pdf.
20. Coppola, E. et al. A first-of-its-kind multi-model convection permitting ensemble for investigating convective phenomena over Europe and the Mediterranean. *Clim. Dyn.* **55**, 3–34. https://doi.org/10.1007/s00382-018-4521-8 (2020).
21. Pontoppidan, M., Reuder, J., Mayer, S. & Kolstad, E. W. Downscaling an intense precipitation event in complex terrain: the importance of high grid resolution. *Tellus A: Dyn. Meteorol. Oceanogr.* **69**(1), 1271561 (2017).
22. Rajczak, J., Kotlarski, S., Salzmann, N. & Schär, C. Robust climate scenarios for sites with sparse observations: a two-step bias correction approach. *Int. J. Climatol.* **36**, 1226. https://doi.org/10.1002/joc.4417 (2016).
23. Rasmussen, R. et al. High-resolution coupled climate runoff simulations of seasonal snowfall over Colorado: a process study of current and warmer climate. *J. Clim.* **24**(12), 3015–3048 (2011).
24. Wigley, T. M. L. & Jones, P. D. Influences of precipitation changes and direct CO2 effects on streamflow. *Nat. (London).* **314**(6007), 149–152. https://doi.org/10.1038/314149a0 (1985).
25. Kar, K. K., Roy, T., Zipper, S. & Godsey, S. E. Nonlinear trends in signatures characterizing non-perennial US streams. *J. Hydrol.* **635**, 131131 (2024).
26. Rojas, R., Feyen, L., Dosio, A. & Bavera, D. Improving pan-european hydrological simulation of extreme events through statistical bias correction of RCM-driven climate simulations. *Hydrol. Earth Sys Sc.* **15**(8), 2599–2620 (2011).
27. Maraun, D. & Widmann, M. *Statistical Downscaling and Bias Correction for Climate Research* (Cambridge University Press, 2018).
28. Van de Velde, J., De Baets, B., Demuzere, M. & Verhoest, N. E. Comparison of occurrence-bias-adjusting methods for hydrological impact modelling. *Hydrol. Earth Sys. Sc. Dis.* **2020**, 1–35 (2020).
29. Vrac, M., Noël, T. & Vautard, R. Bias correction of precipitation through singularity stochastic removal: because occurrences matter. *J. Geophys. Res. Atmos.* **121**, 5237–5258. https://doi.org/10.1002/2015JD024511 (2016).
30. Argüeso, D., Evans, J. P. & Fita, L. Precipitation bias correction of very high-resolution regional climate models. *Hydrol. Earth Syst. Sc.* **17**, 4379–4388. https://doi.org/10.5194/hess-17-4379-2013 (2013).
31. Mao, G., Vogl, S., Laux, P., Wagner, S. & Kunstmann, H. Stochastic bias correction of dynamically downscaled precipitation fields for Germany through Copula-based integration of gridded observation data. *Hydrol. Earth Sys Sc.* **19**, 1787–1806. https://doi.org/10.5194/hess-19-1787-2015 (2015).
32. Piani, C., Haerter, J. O. & Coppola, E. Statistical bias correction for daily precipitation in regional climate models over Europe. *Theor. Appl. Climatol.* **99**(1–2), 187–192. https://doi.org/10.1007/s00704-009-0134-9 (2009).
33. Vrac, M. et al. Dynamical and statistical downscaling of the French Mediterranean climate: uncertainty assessment. *Nat. Hazards Earth Syst. Sci.* **12**, 2769–2784. https://doi.org/10.5194/nhess-12-2769-2012 (2012).
34. Cannon, A. J., Sobie, S. R. & Murdock, T. Q. Bias correction of GCM precipitation by quantile mapping: how well do methods preserve changes in quantiles and extremes? *J. Clim.* **28**(17), 6938–6959. https://doi.org/10.1175/JCLI-D-14-00754.1 (2015).
35. Schmidli, J., Frei, C. & Vidale, P. L. Downscaling from GCM precipitation: a benchmark for dynamical and statistical downscaling methods. *Int. J. Clim.* **26**(5), 679–689. https://doi.org/10.1002/joc.1287 (2006).
36. J Gutowski, W. et al. Temporal–spatial scales of observed and simulated precipitation in Central U.S. Climate. *Am. Meteorological Soc.* https://doi.org/10.1175/1520-0442(2003)016<3841:tsooas>2.0.co;2 (2003). Available at: https://journals.ametsoc.org/view/journals/clim/16/22/1520-0442_2003_016_3841_tsooas_2.0.co_2.xml. Accessed 25 Oct 2024.
37. Themeßi, M. J., Gobiet, A. & Heinrich, G. Empirical-statistical downscaling and error correction of regional climate models and its impact on the climate change signal. *Clim. Change.* **112**(2), 449–468. https://doi.org/10.1007/s10584-011-0224-4 (2012).
38. François, B., Vrac, M., Cannon, A. J., Robin, Y. & Allard, D. Multivariate bias corrections of climate simulations: which benefits for which losses? *Earth Syst. Dyn.* **11**(2), 537–562 (2020).
39. Casanueva, A. et al. Testing bias adjustment methods for regional climate change applications under observational uncertainty and resolution mismatch. *Atmos. Sci. Lett.* **21**(7). https://doi.org/10.1002/asl.978 (2020).

40. Gutiérrez, J. M. et al. An intercomparison of a large ensemble of statistical downscaling methods over Europe: results from the VALUE perfect predictor cross-validation experiment. *Int. J. Clim.* **39**(9), 3750–3785. https://doi.org/10.1002/joc.5462 (2018).
41. Nahar, J., Johnson, F. & Sharma, A. Assessing the extent of non-stationary biases in GCMs. *J. Hydrol.* **549**, 148–162. https://doi.org/10.1016/j.jhydrol.2017.03.045 (2017).
42. Maraun, D. et al. Precipitation downscaling under climate change: Recent developments to bridge the gap between dynamical models and the end user. *Rev. Geophys.* **48**(3), n/a. https://doi.org/10.1029/2009RG000314 (2010).
43. Maraun, D. B., Correction, Q., Mapping & Downscaling *J. Clim.* **26**(6), 2137–2143. https://doi.org/10.1175/JCLI-D-12-00821.1 (2013).
44. Maraun, D. et al. A framework to validate downscaling approaches for climate change studies. *Earth's Future*. **3**(1), 1–14. https://doi.org/10.1002/2014EF000259 (2015).
45. Panofsky, H. A., Brier, G. W. & Best, W. H. *Some Application of Statistics to Meteorology* (Pennsylvania State University, 1958).
46. Déqué, M. Frequency of precipitation and temperature extremes over France in an anthropogenic scenario: model results and statistical correction according to observed values. *Glob Planet. Change*. **57**(1), 16–26. https://doi.org/10.1016/j.gloplacha.2006.11.030 (2007).
47. Qin, X. & Dai, C. Comparison of different quantile delta mapping schemes in frequency analysis of precipitation extremes over mainland Southeast Asia under climate change. *J. Hydrol.* **606**, 127421 (2022).
48. Ghimire, U., Srinivasan, G. & Agarwal, A. Assessment of rainfall bias correction techniques for improved hydrological simulation. *Int. J. Clim.* **39**(4), 2386–2399. https://doi.org/10.1002/joc.5959 (2019).
49. Ngai, S. T., Tangang, F. & Juneng, L. Bias correction of global and regional simulated daily precipitation and surface mean temperature over Southeast Asia using quantile mapping method. *Glob Planet. Change*. **149**, 79–90 (2017).
50. Pastén-Zapata, E., Jones, J. M., Moggridge, H. & Widmann, M. Evaluation of the performance of Euro-CORDEX Regional Climate models for assessing hydrological climate change impacts in Great Britain: a comparison of different spatial resolutions and quantile mapping bias correction methods. *J. Hydrol.* **584**, 124653. https://doi.org/10.1016/j.jhydrol.2020.124653 (2020).
51. Teutschbein, C. & Seibert, J. Bias correction of regional climate model simulations for hydrological climate-change impact studies: review and evaluation of different methods. *J. Hydrol.* **456–457**, 12–29. https://doi.org/10.1016/j.jhydrol.2012.05.052 (2012).
52. Li, H., Sheffield, J. & Wood, E. F. Bias correction of monthly precipitation and temperature fields from Intergovernmental Panel on Climate Change AR4 models using equidistant quantile matching. *J. Geophys. Res. Atmos.* **115**, D10101. https://doi.org/10.1029/2009JD012882 (2010).
53. Miao, C., Su, L., Sun, Q. & Duan, Q. A nonstationary bias-correction technique to remove bias in GCM simulations. *J. Geophys. Res. Atmos.* **121**, 5718–5735. https://doi.org/10.1002/2015JD024159 (2016).
54. Wang, L. & Chen, W. A CMIP5 multimodel projection of future temperature, precipitation, and climatological drought in China. *Int. J. Clim.* **34**(6), 2059–2078 (2014).
55. Buser, C. M., Künsch, H. R., Lüthi, D., Wild, M. & Schär, C. Bayesian multi-model projection of climate: bias assumptions and interannual variability. *Clim. Dyn.* **33**(6), 849–868. https://doi.org/10.1007/s00382-009-0588-6 (2009).
56. Meehl, G. A. et al. *Global Climate Projections. Chapter 10* (Cambridge University Press, 2007).
57. Milly, P. C. D. et al. Stationarity is dead: Whither water management? *Science*. **319**, 573–574. https://doi.org/10.1126/science.1151915 (2008).
58. Gudmundsson, L., Bremnes, J. B., Haugen, J. E. & Engen-Skaugen, T. Technical note: Downscaling RCM precipitation to the station scale using statistical transformations-A comparison of methods. *Hydrol. Earth Sys Sc.* **16**(9), 3383–3390. https://doi.org/10.5194/hess-16-3383-2012 (2012).
59. Michelangeli, P. A., Vrac, M. & Loukos, H. Probabilistic downscaling approaches: Application to wind cumulative distribution functions. *Geophys. Res. Lett.* **36**(11), n/a. https://doi.org/10.1029/2009GL038401 (2009).
60. Maraun, D. Nonstationarities of regional climate model biases in European seasonal mean temperature and precipitation sums. *Geophys. Res. Lett.* **39**(6), n/a. https://doi.org/10.1029/2012GL051210 (2012).
61. Reifen, C. & Ralf, T. Climate projections: Past performance no guarantee of future skill?. *Geoph. Res. Let.* **36**(13), n/a (2009).
62. Papalexiou, S. M., Koutsoyiannis, D. & Makropoulos, C. How extreme is extreme? An assessment of daily rainfall distribution tails. *Hydrol. Earth Syst. Sci.* **17**, 851–862. https://doi.org/10.5194/hess-17-851-2013 (2013).
63. Van de Velde, J., Demuzere, M., De Baets, B. & Verhoest, N. E. Impact of bias nonstationarity on the performance of uni-and multivariate bias-adjusting methods: a case study on data from Uccle, Belgium. *Hydro Earth Syst. Sc.* **26**(9), 2319–2344 (2022).
64. Millares, A. & Moñino, A. Hydro-meteorological drivers influencing suspended sediment transport and yield in a semi-arid mountainous basin. *Earth Surf. Process. Landf.* **45**(15), 3791–3807 (2020).
65. Herrero, J., Polo, M. J., Moñino, A. & Losada, M. A. An energy balance snowmelt model in a Mediterranean site. *J. Hydrol.* **371**(1), 98–107. https://doi.org/10.1016/j.jhydrol.2009.03.021 (2009).
66. Hunter, J. D. & Matplotlib A 2D Graphics Environment. *Comp. Sci. Eng.* **9**(3), 90–95 (2007).
67. IGN. Digital Terrain Model with 25-metre grid pitch (DTM25) of Spain. MDT25. Available online: (2015). https://www.idee.es/csw-inspire-idee/srv/spa/catalog.search?#/metadata/spaignMDT25 (Accessed 31 Jul 2024).
68. DERA. Spatial Reference Data of Andalusia. Available online: https://www.juntadeandalucia.es/institutodeestadisticaycartografia/dega/datos-espaciales-de-referencia-de-andalucia-dera (Accessed on 31 July 2024).
69. Giorgi, F. & Lionello, P. Climate change projections for the Mediterranean region. *Glob Planet. Change*. **63**(2), 90–104. https://doi.org/10.1016/j.gloplacha.2007.09.005 (2008).
70. Jacob, D. et al. EURO-CORDEX: new high-resolution climate change projections for European impact research. *Reg. Environ. Change*. **14**(2), 563–578. https://doi.org/10.1007/s10113-013-0499-2 (2014).
71. Millares, A. & Moñino, A. Sediment yield and transport process assessment from reservoir monitoring in a semi-arid mountainous river. *Hydrol. Process.* **32**(19), 2990–3005 (2018).
72. López-Moreno, J. I., Goyette, S. & Beniston, M. Climate change prediction over complex areas: spatial variability of uncertainties and predictions over the pyrenees from a set of regional climate models. *Int. J. Clim.* **28**, 1535–1550 (2008).
73. Millares, A., Polo, M. J. & Losada, M. A. The hydrological response of baseflow in fractured mountain areas. *Hydrol. Earth Sys Sc.* **13**(7), 1261–1271 (2009).
74. Bergillos, R. J., Rodríguez-Delgado, C., Millares, A., Ortega-Sánchez, M. & Losada, M. A. Impact of river regulation on a Mediterranean delta: Assessment of managed versus unmanaged scenarios. *Water Resour. Res.* **52**(7), 5132–5148 (2016).
75. Moreno-Llorca, R. et al. Multi-scale evolution of ecosystem services' supply in Sierra Nevada (Spain): an assessment over the last half-century. *Ecosyst. Serv.* **46**, 101204. https://doi.org/10.1016/j.ecoser.2020.101204 (2020).
76. Polo, M. J. et al. Snow dynamics, hydrology, and erosion. In The Landscape of the Sierra Nevada: A Unique Laboratory of Global Processes in Spain. 149–164 (Springer International Publishing, (2022).
77. IPCC,2014 Climate Change. in *Synthesis Report. Contribution of Working Groups I, II and III to the Fifth Assessment Report of the Intergovernmental Panel on Climate Change [Core Writing Team*. 151 (eds Pachauri, R. K. & Meyer, L. A.) (IPCC, 2014).
78. IPCC. : Summary for policymakers. In: *Climate Change 2023: Synthesis Report.*Contribution of Working Groups I, II and III to the Sixth Assessment Report of the Intergovernmental Panel on Climate Change [Core Writing Team, H. Lee, and J. Romero (eds.)]. IPCC, Geneva, Switzerland, 1–34, doi:https://doi.org/10.59327/IPCC/AR6-9789291691647.001. (2023).
79. Sobolowski, S. et al. EURO-CORDEX CMIP6 GCM selection & Ensemble Design: best practices and recommendations. *Zenodo*. https://doi.org/10.5281/zenodo.7673400 (2023).

80. Vazifehkhah, S. & Kahya, E. Performance evaluation of CORDEX precipitation series on a basin scale. In *8th Atmospheric Sciences Symposium; ATMOS2017* (2017).
81. Georgoulias, A. K. et al. Climate change projections for Greece in the 21st century from high-resolution EURO-CORDEX RCM simulations. *Atmos. Res.* **271**, 106049 (2022).
82. Cobos, M., Otiñar, P., Magaña, P. & Baquerizo, A. A method to characterize climate, earth, or environmental vector random processes. *Stoch. Env Res. Risk A.* **36**, 4073–4085. https://doi.org/10.1007/s00477-022-02260-9 (2022).
83. Solari, S. & Losada, M. A. Non-stationary wave height climate modeling and simulation. *J. Geoph. Res.* **116**(C9), n/a. https://doi.org/10.1029/2011JC007101 (2011).
84. Solari, S. & Losada, M. A. Unified distribution models for met-ocean variables: application to series of significant wave height. *Coast Eng.* **68**, 67–77 (2012).
85. Ines, A. V. M. & Hansen, J. W. Bias correction of daily GCM rainfall for crop simulation studies. *Agric. For. Meteorol.* **138**(1), 44–53. https://doi.org/10.1016/j.agrformet.2006.03.009 (2006).
86. Jiang, P., Yu, Z., Gautam, M. R., Yuan, F. & Acharya, K. Changes of storm properties in the United States: observations and multimodel ensemble projections. *Glob Planet. Change.* **142**, 41–52 (2016).
87. Wilcke, R. A. I., Mendlik, T. & Gobiet, A. Multi-variable error correction of regional climate models. *Clim. Change.* **120**(4), 871–887. https://doi.org/10.1007/s10584-013-0845-x (2013).
88. Kjellström, E. et al. Daily and monthly temperature and precipitation statistics as performance indicators for regional climate models. *Clim. Res.* **44**(2/3), 135–150. https://doi.org/10.3354/cr00932 (2010).
89. Hagemann, S. et al. Evaluation of water and energy budgets in regional climate models applied over Europe. *Clim. Dyn.* **23**, 547–567 (2004).
90. Cobos, M., Otiñar, P., Magaña, P., Loarca, A., Baquerizo, A. & L., & Marinetools. Temporal: a python package to simulate earth and environmental time series. *Enviro Model. Softw.* **150**(105), 359 (2022).
91. Tong, Y., Gao, X., Han, Z., Xu, Y. & Giorgi, F. Bias correction of temperature and precipitation over China for RCM simulations using the QM and QDM methods. *Clim. Dyn.* **57**, 1425–1443 (2021).
92. btschwertfeger Schwertfeger, B. python-cmethods: v2.0.2 (v2.0.2). *Zenodo*. https://doi.org/10.5281/zenodo.10610876 (2014).
93. Ban, N. et al. The first multi-model ensemble of regional climate simulations at kilometer-scale resolution, part I: evaluation of precipitation. *Clim. Dyn.* **57**, 275–230. https://doi.org/10.1007/s00382-021-05708-w (2021).
94. Sangelantoni, L., Russo, A. & Gennaretti, F. Impact of bias correction and downscaling through quantile mapping on simulated climate change signal: a case study over Central Italy. *Theor. Appl. Climatol.* **135**(1–2), 725–740. https://doi.org/10.1007/s00704-018-2406-8 (2019).
95. Lange, S. Trend-preserving bias adjustment and statistical downscaling with ISIMIP3BASD (v1.0). *Geosci. Model. Dev.* **12**, 3055–3070. https://doi.org/10.5194/gmd-12-3055-2019 (2019).
96. Ehret, U., Zehe, E., Wulfmeyer, V., Warrach-Sagi, K. & Liebert, J. Should we apply bias correction to global and regional climate model data? *Hydrol. Earth Syst. Sci.* **16**, 3391–3404. https://doi.org/10.5194/hess-16-3391-2012 (2012).
97. Yao, J., Yang, Q., Mao, W., Zhao, Y. & Xu, X. Precipitation trend–elevation relationship in arid regions of China. *Glob Planet. Change.* **143**, 1–9 (2016).
98. Majhi, A., Dhanya, C. T. & Chakma, S. Quantification of model uncertainty in sub-daily extreme precipitation projections. *Glob Planet. Change.* **218**, 103967 (2022).
99. Reyers, M., Pinto, J. G. & Paeth, H. Statistical–dynamical downscaling of present day and future precipitation regimes in the Aksu river catchment in Central Asia. *Glob Planet. Change.* **107**, 36–49 (2013).
100. Rizou, D., Flocas, H. A., Athanasiadis, P. & Bartzokas, A. Relationship between the Indian summer monsoon and the large-scale circulation variability over the Mediterranean. *Atmos. Res.* **152**, 159–169 (2015).
101. Lira-Loarca, A. L., Cobos, M., Besio, G. & Baquerizo, A. Projected wave climate temporal variability due to climate change. *Stoch. Environ. Res. Risk Assess.* **35**(9), 1741–1757. https://doi.org/10.1007/s00477-020-01946-2 (2021).
102. Kouhestani, S., Eslamian, S. S., Abedi-Koupai, J. & Besalatpour, A. A. Projection of climate change impacts on precipitation using soft-computing techniques: a case study in Zayandeh-Rud Basin, Iran. *Glob Planet. Change.* **144**, 158–170 (2016).

Acknowledgements

This work was supported by (1) the European Regional Development Fund (ERDF) through the project RISK-COAST (SOE3/P4/E0868), "Desarrollo de herramientas para prevenir y gestionar los riesgos geológicos en la costa ligados al cambio climático" of the European Interreg SUDOE Program, (2) FEDER/Junta de Andalucía-Consejería de Transformación Económica, Industria, Conocimiento y Universidades through ARCA project (B-TEP-110-UGR20), (3) EPICOS (Plan Andaluz de Investigación, Desarrollo e Innovación, PAIDI 2020. Ref. ProyExcel_00375), (4) Work of the study of flooding and erosion in coastal areas of Andalusia in a climate change scenario (CONTR2018/66984), and (5) the UGR's Own Plan and the Excellence Units Program. It has also received funding under the Life Watch-ERIC infrastructure (LifeWatch-2019-10-UGR-01; FEDER-Multiregional Operational Program for Spain). M.C. is indebted to Consejería de Transformación Económica, Industria, Conocimiento y Universidades de la Junta de Andalucía (POSTDOC_ 21_00724) which partially funded his work.

Authors' contributions

M.C.I. and M.C.B. (corresponding author) made the data curation, developed the methodology, coded the scripts, prepared the figures, and wrote the main manuscript text. A.M. and A.B. developed the methodology and review the manuscript.

Declarations

Competing interests

The authors declare no competing interests.

Additional information

Supplementary Information The online version contains supplementary material available at https://doi.org/10.1038/s41598-024-76848-2.

Correspondence and requests for materials should be addressed to M.C.